Journal of Power Sources 220 (2012) 430–448

Contents lists available at SciVerse ScienceDirect

Journal of Power Sources

journal homepage: www.elsevier.com/locate/jpowsour

# One-dimensional physics-based reduced-order model of lithium-ion dynamics

James L. Lee [a], Andrew Chemistruck [b], Gregory L. Plett [a,*]

[a] Department of Electrical and Computer Engineering, University of Colorado Colorado Springs, Colorado Springs, CO 80918, United States
[b] Texas Instruments, 2900 Semiconductor Dr., Santa Clara, CA 95051-0695, United States

## HIGHLIGHTS

- We derive a reduced-order discrete-time state-space model of a lithium-ion cell.
- We start with known Laplace-domain transfer functions of the porous-electrode model.
- Then, we derive transfer functions for electrolyte concentration and the potentials.
- Using the discrete-time realization algorithm, we produce a reduced-order model.
- A fifth-order model can accurately model a dynamic drive cycle.

## ARTICLE INFO

*Article history:*
Received 2 April 2012
Received in revised form
14 June 2012
Accepted 26 July 2012
Available online 4 August 2012

*Keywords:*
Lithium ion battery
Electrochemical model
Battery management systems
Distributed parameter model order reduction
Transcendental transfer function model order reduction

## ABSTRACT

We present a method to produce a physics-based one-dimensional discrete-time state-space reduced-order model (ROM) of a lithium-ion cell. The resulting ROM can predict the five variables of a standard porous-electrode model—reaction flux, solid and electrolyte lithium concentration, and solid and electrolyte potentials—at any location across the cell cross section, as well as cell terminal voltage. The method to generate the model involves first linearizing the porous-electrode-model equations, and then deriving closed-form Laplace-domain transfer functions from the linearized equations. Next, the discrete-time realization algorithm (DRA) is used to convert the transfer functions into an optimal discrete-time state-space realization. Advantages of this approach include that the DRA avoids nonlinear optimization and gives a straightforward method for selecting the system order for the ROM. Simulation results demonstrate that the ROM cell voltage predictions and the ROM internal electrochemical variable predictions match very closely with results obtained by simulating the full nonlinear porous-electrode partial differential equations.



## 1. Introduction

An important requirement for a battery management system is that it be able to compute accurate estimates of a number of fundamental quantities that describe the present status of the battery pack's cells. These include: state-of-charge (SOC), state-of-health (usually comprising a cell resistance and/or capacity estimate), state-of-life, available energy, available power, and time-to-empty. The best available methods to compute these estimates require high-fidelity but computationally simple mathematical models of battery cell input/output (current/voltage) dynamics. Furthermore, we believe that future battery-management-system requirements will necessitate models that give insight into cell internal electrochemical dynamics; for example, to predict and to minimize degradation mechanisms, to slow aging.

Broadly speaking, battery models that might be used in such model-based estimators fall into two categories: (1) empirical equivalent-circuit type models, and (2) physics-based models. Equivalent-circuit models (ECMs) are formulated by recognizing that cell current/voltage behavior is often well approximated by a model that uses a voltage source, resistors, capacitors, and Warburg impedances as analogs to observed behaviors in the cell [1]. The values of the model components are found via empirical system-identification approaches, based on lab-generated cell-test data. Present battery-management-system algorithms rely almost exclusively on ECMs due to the simplicity and robustness of these models, which allow them to operate in real-time embedded applications. However, ECMs do not provide insight into the electrochemical dynamics that occur internal to the cell during

* Corresponding author. Tel.: +1 719 255 3468; fax: +1 719 255 3589.
*E-mail addresses:* jlee3@uccs.edu (J.L. Lee), andy.chemistruck@ti.com (A. Chemistruck), gplett@uccs.edu, glp@eas.uccs.edu (G.L. Plett).

0378-7753/$ – see front matter © 2012 Elsevier B.V. All rights reserved.
http://dx.doi.org/10.1016/j.jpowsour.2012.07.075

operation, and this insight will be key to fully utilizing the cell without causing premature degradation.

Alternately, physics-based models, originally developed by Doyle, Fuller, and Newman [2,3], give equations that provide full information on the internal electrochemical dynamics of the cell. However, the coupled partial-differential equations (PDEs) that form the model result in computational complexity that makes their use in real-time embedded battery-management applications impractical. For real-time control applications, we desire the best features of the ECMs and the physics-based models; namely, we need a computationally simple and robust reduced-order model (ROM) of cell dynamics that predicts not only the cell voltage and SOC of the cell during operation, but also accurate estimates of the cell's internal electrochemical variables.

A number of approaches to reduce the computational complexity of the physics-based models have been explored in the literature. The primary gains have been made by observing that much of the computational complexity involved in solving the rigorous physics-based model equations comes from solving for the concentration of lithium in the solid particles of the electrodes. Many methods therefore focus on making approximations to simplify this computation. Both Wang et al. [4] and Subramanian et al. [5] have used a parabolic profile to estimate the concentration throughout the solid particle, eliminating the need for this PDE. This approach works at low discharge rates but does not perform well for highly dynamic current inputs such as those encountered in hybrid- and electric-vehicle applications. Others have used the Padé approximation to match the power series representation of the solid diffusion equation to a desired order [6]. The Padé approximation matches the dc values but also does not perform as well at higher frequencies. Cai and White use proper orthogonal decomposition [7] to find the electrochemical variables at discrete locations within the solid particle and across the 1D cell. This method accurately models the cell behavior at high currents but requires either existing experimental data or simulation results to generate the ROM. As cell parameters change due to aging, we desire a method that does not require offline simulation results in order to generate an updated ROM.

In our opinion, the most promising approach to reduced-order modeling has been introduced by Smith et al. [8,9]. In this work, they showed how to linearize the coupled PDEs of the rigorous pseudo-2D porous-electrode model and derive analytic Laplace-domain transfer functions from the linearized model. They were able to model several internal cell electrochemical variables at different spatial locations within the cell this way: reaction flux $j(z,t)$, solid-electrolyte potential difference $\phi_{s-e}(z,t)$, overpotential $\eta(z,t)$, and solid particle surface concentration $c_{s,e}(z,t)$. They did not derive an analytic transfer function for the concentration of lithium in the electrolyte $c_e(x,t)$; as an alternative, they used the finite element method to solve for this variable.

Smith et al. then used a nonlinear optimization routine to fit a reduced-order model to these transfer functions in such a way as to minimize the error between the frequency-domain response of the reduced-order model and the full-order linear transfer-function model. In principle, this nonlinear optimization step can work well. In practice, however, it often does not. The results of nonlinear optimization are very sensitive to the initial starting estimate, they are not guaranteed to be globally optimal, are not guaranteed to converge in bounded time, and the model order must be found via trial and error. Nonlinear optimization is not well suited for unsupervised operation in embedded systems, which limits its applicability in fielded battery-management applications where the parameters of the transfer functions, and hence the ROM itself, may need to adapt as the cell ages.

In this paper, we propose an improvement to this approach. We begin, as did Smith and colleagues, by finding transfer functions of the cell variables of interest. However, we remove the problematic nonlinear optimization step and instead find the reduced-order model using the discrete-time realization algorithm (DRA) [10], which overcomes the major disadvantages listed above. Namely, the DRA computes a discrete-time state-space model directly from transfer functions, without requiring an initial guess of the reduced-order model parameters, while yielding a globally optimal result in bounded time, and also supplying guidance to choosing the order of the reduced-order model. In [10], Lee et al. demonstrate the DRA on a single-input single-output system. Here, we show how to use the method to form a single-input multiple-output cell model. Additionally, we extend the model of Smith et al. by deriving analytic transfer functions for the solid potential, $\phi_s(z,t)$, electrolyte potential, $\phi_e(x,t)$, and $c_e(x,t)$. We also modify their derivation steps somewhat to allow for a particle surface-film resistance $R_{film}$ in the Butler–Volmer equation, and we propose nonlinear output corrections that improve the accuracy over a strictly linear model.

This paper is the second in a series of planned works. The first paper in the series introduced the DRA as a method for converting a transcendental transfer function into an optimal discrete-time state-space reduced-order model [10]. This is the second paper in the series, which shows how to find transcendental transfer functions corresponding to lithium-ion internal cell dynamics. The scope of the work in this paper is limited to showing how to create a ROM that is linearized to give accurate predictions around a single SOC and temperature set-point only. A planned third paper in this series will show how to enhance the method presented herein to allow wide variations in temperature and SOC.

This paper is organized in the following way. In Section 2, we reproduce the five equations of the standard pseudo-2D porous-electrode model. We then derive transfer functions for the electrode variables $j(z,t)$, $\eta(z,t)$, $c_{s,e}(z,t)$, and $\phi_s(z,t)$ using a methodology similar to that in [8,9], but which is modified to allow the addition of a particle surface-film resistance. We then show how to model the electrolyte variables $\phi_e(x,t)$ and $c_e(x,t)$ as transfer functions. In Section 3, we briefly review the DRA and show how to use it to yield optimal reduced-order discrete-time state-space realization of these transfer functions. In Section 4, we describe how the model's voltage estimates can be improved over purely linear estimates by adding nonlinear output corrections. Results are presented in Section 5 where we compare predictions from our reduced-order model to those computed using the PDEs of the rigorous pseudo-2D model.

## 2. Derivation of transfer functions of reduced-order model

In this section, we derive transfer functions corresponding to linearized equations of the internal electrochemical dynamics of a cell. The derivation is quite long; however, the final reduced-order model produced using these transfer functions is computationally very simple—similar to the complexity of an ECM. Furthermore, the transfer functions are capable of very accurate predictions of internal cell electrochemical states and also cell terminal voltage.

### 2.1. Pseudo-2D porous-electrode model of cell

We begin by presenting the partial differential equations, boundary conditions and initial conditions that comprise the pseudo-2D porous-electrode cell model developed by Doyle, Fuller and Newman [2,3], which is the starting point to our derivation. We reproduce these equations because everything that follows depends on their exact form, and variations in how these equations

are presented in the literature might otherwise introduce an ambiguity that results in substantial confusion.

The pseudo-2D porous-electrode cell model is written in terms of the electrochemical variables that summarize the internal state of a cell during operation. Specifically, they model electrode-scale variables: reaction flux $j$, potential in the solid phase $\phi_s$, and concentration of lithium in the solid phase $c_s$. They also model cell-scale variables: potential in the electrolyte phase $\phi_e$ and concentration of lithium in the electrolyte phase $c_e$.

Solid particles in the electrodes are modeled as spheres with radius $R_s$. The concentration of lithium in these particles $c_s(r,x,t)$ is assumed to be radially symmetric within any given particle, so overall is a function of the radial distance $r$ from the center of the particle as well as the spatial location $x$ of the particle along the one-dimensional cross-section across the cell ($x = 0$ at the negative current collector and $x = L$ at the positive current collector). Lithium in the solid is assumed to move via diffusion:

$$\frac{\partial c_s(r,x,t)}{\partial t} = \frac{D_s}{r^2}\frac{\partial}{\partial r}\left(r^2\frac{\partial c_s(r,x,t)}{\partial r}\right). \tag{1}$$

The boundary conditions to this PDE are

$$D_s\frac{\partial c_s(0,x,t)}{\partial r} = 0, \quad \text{and} \quad D_s\frac{\partial c_s(R_s,x,t)}{\partial r} = -j(x,t),$$

where the reaction flux $j(x,t)$ is a measure of the amount of lithium moving across the boundary of the solid particle. The initial concentration profile of lithium in the particle is

$$c_s(r,x,0) = c_{s,0}, \quad 0 \le r \le R_s.$$

Concentration of lithium in the electrolyte $c_e(x,t)$ is derived from the principle of mass conservation, and is found to be

$$\frac{\partial(\varepsilon_e c_e(x,t))}{\partial t} = \frac{\partial}{\partial x}\left(D_e^{\text{eff}}\frac{\partial}{\partial x}c_e(x,t)\right) + \left(1-t_+^0\right)a_s j(x,t), \tag{2}$$

where the boundary conditions are given by

$$\frac{\partial c_e(0,t)}{\partial x} = \frac{\partial c_e(L,t)}{\partial x} = 0.$$

The initial concentration of lithium in the electrolyte is $c_e(x,0) = c_{e,0}$ for $0 \le x \le L$.

Conservation of charge in the solid phase gives the equation for the potential in the solid phase $\phi_s(x,t)$, which is

$$\frac{\partial}{\partial x}\left(\sigma^{\text{eff}}\frac{\partial}{\partial x}\phi_s(x,t)\right) - a_s F j(x,t) = 0, \tag{3}$$

with boundary conditions

$$-\sigma^{\text{eff}}\frac{\partial\phi_s(0,t)}{\partial x} = \sigma^{\text{eff}}\frac{\partial\phi_s(L,t)}{\partial x} = \frac{I}{A} = i_{\text{app}}.$$

Conservation of charge in the electrolyte phase gives the equation for the potential of the electrolyte phase $\phi_e(x,t)$, which is

$$\frac{\partial}{\partial x}\left(\kappa^{\text{eff}}\frac{\partial}{\partial x}\phi_e(x,t)\right) + \frac{\partial}{\partial x}\left(\kappa_D^{\text{eff}}\frac{\partial}{\partial x}\ln c_e(x,t)\right) + a_s F j(x,t) = 0, \tag{4}$$

where $\kappa^{\text{eff}} = \kappa\varepsilon_e^{\text{brug}}$ and

$$\kappa_D^{\text{eff}} = \frac{-2RT}{F}\kappa^{\text{eff}}\left(1-t_+^0\right)\left(1+\frac{d\ln f_\pm}{d\ln c_e}\right),$$

with the boundary conditions

$$\frac{\partial\phi_e(0,t)}{\partial x} = \frac{\partial\phi_e(L,t)}{\partial x} = 0.$$

In this work we assume the value for $d\ln f_\pm/d\ln c_e$ is set to 0.

Finally, the Butler–Volmer equation gives the reaction flux $j(x,t)$ at different points in the electrodes

$$j(x,t) = kc_e^{1-\alpha}(c_{\max}-c_{s,e})^{1-\alpha}c_{s,e}^{\alpha} \times \left(\exp\left(\frac{(1-\alpha)F}{RT}\eta\right) - \exp\left(-\frac{\alpha F}{RT}\eta\right)\right), \tag{5}$$

where the overpotential $\eta$ is

$$\eta = \phi_s - \phi_e - U_{\text{ocp}} - jFR_{\text{film}}. \tag{6}$$

Eqs. (1)–(5) comprise the pseudo-2D porous-electrode model. The main dimension is the cross-sectional distance $x$ across the cell; the pseudo dimension is the radial distance $r$ into a particular electrode particle. Similar to Smith et al., we eliminate the need for computing the pseudo dimension $r$ by using transfer-function methods. We then show how to compute transfer functions for the cell variables at any desired set of $x$ locations across the cell.

### 2.2. Transfer functions for reaction flux $j(z,t)$, overpotential $\eta(z,t)$, and solid surface concentration $c_{s,e}(z,t)$

We begin by finding transfer functions for three cell variables that are very tightly coupled together: the reaction flux $j(z,t)$, the overpotential $\eta(z,t)$, and the solid surface concentration $c_{s,e}(z,t)$. Note the introduction of the dimensionless spatial variable $z$, which is defined only within the electrodes and not within the separator. In the negative electrode, $z = x/L_n$ and in the positive electrode, $z = (L-x)/L_p$. In both cases, $z = 0$ at the outer current collector/electrode interface and $z = 1$ at the inner electrode/separator interface. This is illustrated in Fig. 1, which shows the set of variables that exist in each domain of the cell's cross section, and whether the variable's position variable is generally chosen to be $x$ or $z$.

We embark on the derivation of these three linear transfer functions from the porous-electrode equations in a manner largely similar to that of Smith et al. [8,9], although we approach the linearization differently in order to add a particle surface film resistance term $R_{\text{film}}$ to the Butler–Volmer equation. We make the same fundamental two assumptions as [8,9]: (1) we assume linear behavior and enforce that linear behavior by linearizing nonlinear expressions as needed, and (2) we assume that reaction flux can be decoupled from electrolyte concentration, which is equivalent to assuming that electrolyte potential is independent of electrolyte concentration when deriving the transfer function for reaction flux.

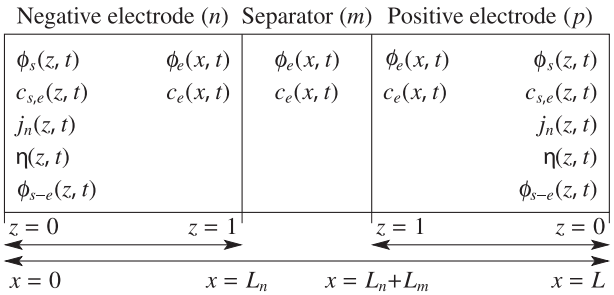


**Fig. 1.** Schematic diagram of cell showing variables that exist in each domain and the orientation of $z$ in the electrodes.

We start with Assumption 1, and linearize the Butler–Volmer equation around the set-point $p^*$ defined as

$$p^* = \{c_{s,e} = c_{s,0}, c_e = c_{e,0}, \phi_{s-e} = U_{ocp}(c_{s,0}), j = 0\},$$

where we have defined $\phi_{s-e} = \phi_s - \phi_e$. Re-arranging Eq. (5) gives

$$\frac{j}{kc_e^{1-\alpha}(c_{max}-c_{s,e})^{1-\alpha}c_{s,e}^{\alpha}} = \exp\left(\frac{(1-\alpha)F}{RT}\eta\right) - \exp\left(-\frac{\alpha F}{RT}\eta\right). \quad (7)$$

Approximating the left-hand-side (LHS) of Eq. (7) with the first two terms of its Taylor-series expansion gives

$$\begin{aligned} LHS &\approx LHS(p^*) + \left.\frac{\partial LHS}{\partial c_{s,e}}\right|_{p^*}(c_{s,e}-c_{s,0}) \\ &\quad + \left.\frac{\partial LHS}{\partial c_e}\right|_{p^*}(c_e - c_{e,0}) + \left.\frac{\partial LHS}{\partial j}\right|_{p^*} j \\ &= 0 + 0\times(c_{s,e}-c_{s,0}) + 0\times(c_e - c_{e,0}) \\ &\quad + \frac{j}{kc_{e,0}^{1-\alpha}(c_{max}-c_{s,0})^{1-\alpha}c_{s,0}^{\alpha}} \\ &= j/j_0, \end{aligned} \quad (8)$$

where $j_0 = kc_{e,0}^{1-\alpha}(c_{max}-c_{s,0})^{1-\alpha}c_{s,0}^{\alpha}$. Similarly, we expand $\eta$ in the right-hand-side (RHS) of Eq. (7) using Eq. (6), and approximate it with the first two terms of its Taylor-series expansion to get

$$\begin{aligned} RHS &= \exp\left(\frac{(1-\alpha)F}{RT}\left(\phi_{s-e} - U_{ocp} - FR_{film}j\right)\right) \\ &\quad - \exp\left(-\frac{\alpha F}{RT}\left(\phi_{s-e} - U_{ocp} - FR_{film}j\right)\right) \\ &\approx \mathrm{RHS}\left(p^*\right) + \left.\frac{\partial \mathrm{RHS}}{\partial c_{s,e}}\right|_{p^*}(c_{s,e}-c_{s,0}) \\ &\quad + \left.\frac{\partial \mathrm{RHS}}{\partial \phi_{s-e}}\right|_{p^*}(\phi_{s-e} - U_{ocp}(c_{s,0})) + \left.\frac{\partial \mathrm{RHS}}{\partial j}\right|_{p^*} j \\ &= 0 + \frac{F}{RT}(\phi_{s-e} - U_{ocp}(c_{s,0})) \\ &\quad - \frac{F}{RT}\left[\left.\frac{\partial U_{ocp}}{\partial c_{s,e}}\right|_{c_{s,0}}\right](c_{s,e}-c_{s,0}) - \frac{F^2R_{film}}{RT}j. \end{aligned} \quad (9)$$

We now remove the constant bias from $\phi_{s-e}$ and $c_{s,e}$ by defining debiased versions as $\tilde{\phi}_{s-e} = \phi_{s-e} - U_{ocp}(c_{s,0})$ and $\tilde{c}_{s,e} = c_{s,e} - c_{s,0}$, where the tilde "~" decoration is used throughout this paper to refer to a debiased variable. We substitute these debiased variables into our results, and set Eq. (8) equal to Eq. (9) to arrive at the linearized Butler–Volmer equation

$$\frac{j}{j_0} = \frac{F}{RT}\tilde{\phi}_{s-e} - \frac{F}{RT}\left[\left.\frac{\partial U_{ocp}}{\partial c_{s,e}}\right|_{c_{s,0}}\right]\tilde{c}_{s,e} - \frac{F^2R_{film}}{RT}j. \quad (10)$$

Rearranging Eq. (10) to solve for $\tilde{\phi}_{s-e}$ gives

$$\tilde{\phi}_{s-e} = F\left(R_{ct} + R_{film}\right)j + \left[\left.\frac{\partial U_{ocp}}{\partial c_{s,e}}\right|_{c_{s,0}}\right]\tilde{c}_{s,e},$$

where we define the charge-transfer resistance as $R_{ct} = RT/(j_0F^2)$. We can further condense notation by defining $R_{tot}$=$R_{ct} + R_{film}$ to get

$$\tilde{\phi}_{s-e}(z,t) = FR_{tot}j(z,t) + \left[\left.\frac{\partial U_{ocp}}{\partial c_{s,e}}\right|_{c_{s,0}}\right]\tilde{c}_{s,e}(z,t). \quad (11)$$

We leave this result to the side for the time being and now focus on the solid surface concentration. We define $c_{s,e}(z,t) = c_s(R_s,z,t)$, and corresponding debiased versions

$$\tilde{c}_{s,e}(z,t) = \tilde{c}_s(R_s,z,t) = c_s(R_s,z,t) - c_{s,0}. \quad (12)$$

Eq. (1), modified to be written in terms of the debiased variable, is

$$\frac{\partial \tilde{c}_s(r,z,t)}{\partial t} = \frac{D_s}{r^2}\frac{\partial}{\partial r}\left(r^2\frac{\partial \tilde{c}_s(r,z,t)}{\partial r}\right),$$

with boundary and initial conditions

$$D_s\frac{\partial \tilde{c}_s(0,z,t)}{\partial r} = 0, \quad \text{and} \quad D_s\frac{\partial \tilde{c}_s(R_s,z,t)}{\partial r} = -j(z,t),$$

$$\tilde{c}_s(r,z,0) = 0, \quad 0 \le r \le R_s.$$

A transfer-function solution to this partial differential equation was derived by Jacobsen and West [11], and is

$$\frac{\tilde{C}_{s,e}(s)}{J(s)} = \frac{R_s}{D_s}\left(\frac{\tanh(\beta)}{\tanh(\beta)-\beta}\right), \quad (13)$$

where $\beta = R_s\sqrt{s/D_s}$.

We will now use the two results found to this point, Eqs. (11) and (13), to derive a transfer function for $\phi_{s-e}$. We initially focus on the negative electrode only, and later generalize to the positive electrode as well. In the normalized $z$ dimension, the solid potential equation (Eq. (3)) is written as

$$\frac{\sigma^{eff}}{L_n^2}\frac{\partial^2}{\partial z^2}\phi_s = a_sFj, \quad (14)$$

with boundary conditions $((\sigma^{eff}/L_n)(\partial\phi_s/\partial z))\big|_{z=0} = -i_{app}/A$ and $(\partial\phi_s/\partial z)|_{z=1} = 0$. The potential in the electrolyte is

$$\frac{\kappa^{eff}}{L_n^2}\frac{\partial^2}{\partial z^2}\phi_e = -a_sFj, \quad (15)$$

where Assumption 2 is used to omit the electrolyte-concentration dependent term from the left-hand side of Eq. (4) and where a linearized $\kappa^{eff}$ is defined as $\kappa(c_{e,0})\varepsilon_e^{brug}$ in the transfer function models only. The boundary conditions are $(\partial\phi_e(z,t)/\partial z)|_{z=0} = 0$ and $(\kappa^{eff}/L_n)(\partial\phi_e(z,t)/\partial z)\big|_{z=1} = i_{app}/A$. Subtracting Eq. (15) from Eq. (14) gives a single equation for the phase potential difference $\phi_{s-e}$

$$\frac{\partial^2}{\partial z^2}\phi_{s-e} = a_sFL_n^2\left(\frac{1}{\sigma^{eff}} + \frac{1}{\kappa^{eff}}\right)j, \quad (16)$$

with boundary conditions $((\sigma^{eff}/L_n)(\partial\phi_{s-e}/\partial z))\big|_{z=0} = ((-\kappa^{eff}/L_n)(\partial\phi_{s-e}/\partial z))\big|_{z=1} = -i_{app}/A$. We take the Laplace transform of Eq. (11)

$$\tilde{\Phi}_{s-e}(z,s) = FR_{tot}J(z,s) + \left[\left.\frac{\partial U_{ocp}}{\partial c_{s,e}}\right|_{c_{s,0}}\right]\tilde{C}_{s,e}(z,s), \quad (17)$$

and then rewrite the rightmost term as

$$\tilde{C}_{s,e}(z,s) = \frac{\tilde{C}_{s,e}(z,s)}{J(z,s)}J(z,s).$$

From Eq. (13), we have a transfer function for $\tilde{C}_{s,e}(s)/J(s)$ at a single spatial location in the electrode. However, note that diffusion happens only along the radial dimension $r$ and not the lateral dimension $z$, so we can write the same transfer function $\tilde{C}_{s,e}(s)/J(s)$ at every $z$ location. In other words,

$\tilde{C}_{s,e}(z,s)/J(z,s) = \tilde{C}_{s,e}(s)/J(s)$ for every value of $z$. Inserting this result into Eq. (17), we get

$$\begin{aligned}\tilde{\Phi}_{s-e}(z,s) &= \left(FR_{tot} + \left[\left.\frac{\partial U_{ocp}}{\partial c_{s,e}}\right|_{c_{s,0}}\right]\frac{\tilde{C}_{s,e}(s)}{J(s)}\right)J(z,s) \\ &= F\left(R_{tot} + \left[\left.\frac{\partial U_{ocp}}{\partial c_{s,e}}\right|_{c_{s,0}}\right]\frac{R_s}{FD_s}\left(\frac{\tanh(\beta)}{\tanh(\beta)-\beta}\right)\right)J(z,s).\end{aligned} \tag{18}$$

Now, writing Eq. (16) in the Laplace domain gives

$$\begin{aligned}\frac{\partial^2\tilde{\Phi}_{s-e}(z,s)}{\partial z^2} &= a_s F L_n^2\left(\frac{1}{\sigma^{eff}}+\frac{1}{\kappa^{eff}}\right)J(z,s) \\ &= a_s L_n^2\left(\frac{1}{\sigma^{eff}}+\frac{1}{\kappa^{eff}}\right)\left(R_{tot} + \left[\left.\frac{\partial U_{ocp}}{\partial c_{s,e}}\right|_{c_{s,0}}\right]\right. \\ &\quad \left.\times\frac{R_s}{FD_s}\left(\frac{\tanh(\beta)}{\tanh(\beta)-\beta}\right)\right)^{-1}\tilde{\Phi}_{s-e}(z,s),\end{aligned}$$

with boundary conditions,

$$\left.\frac{\sigma^{eff}}{L_n}\frac{\partial\tilde{\Phi}_{s-e}(z,s)}{\partial z}\right|_{z=0} = \left.\frac{-\kappa^{eff}}{L_n}\frac{\partial\tilde{\Phi}_{s-e}(z,s)}{\partial z}\right|_{z=1} = \frac{-I_{app}(s)}{A}.$$

For convenience of notation, we define dimensionless variable $\nu(s)$ as[1]

$$\nu(s) = \frac{L_n\sqrt{\frac{a_s}{\sigma^{eff}}+\frac{a_s}{\kappa^{eff}}}}{\sqrt{R_{tot} + \left[\left.\frac{\partial U_{ocp}}{\partial c_{s,e}}\right|_{c_{s,0}}\right]\frac{R_s}{FD_s}\left(\frac{\tanh(\beta)}{\tanh(\beta)-\beta}\right)}}, \tag{19}$$

which allows us to write

$$\frac{\partial^2\tilde{\Phi}_{s-e}(z,s)}{\partial z^2} - \nu^2(s)\tilde{\Phi}_{s-e}(z,s) = 0.$$

The solution to this homogeneous differential equation, after satisfying both boundary conditions, is

$$\begin{aligned}\frac{\tilde{\Phi}_{s-e}(z,s)}{I_{app}(s)} &= \frac{L_n}{A\nu(s)\sinh(\nu(s))}\left(\frac{1}{\kappa^{eff}}\cosh(\nu(s)z)\right. \\ &\quad \left.+\frac{1}{\sigma^{eff}}\cosh(\nu(s)(z-1))\right).\end{aligned} \tag{20}$$

From this result, we find the transfer function for the reaction flux to be

$$\frac{J(z,s)}{I_{app}(s)} = \frac{J(z,s)}{\tilde{\Phi}_{s-e}(z,s)}\frac{\tilde{\Phi}_{s-e}(z,s)}{I_{app}(s)} = \frac{\nu^2(s)}{a_s F L^2\left(\frac{1}{\kappa^{eff}}+\frac{1}{\sigma^{eff}}\right)}\frac{\tilde{\Phi}_{s-e}(z,s)}{I_{app}(s)},$$

where $J(z,s)/\tilde{\Phi}_{s-e}(z,s)$ is found from Eq. (18). Expanding gives

$$\begin{aligned}\frac{J(z,s)}{I_{app}(s)} &= \frac{\nu(s)}{a_s F L_n A\left(\kappa^{eff}+\sigma^{eff}\right)} \\ &\quad\times\left(\frac{\sigma^{eff}\cosh(\nu(s)z)+\kappa^{eff}\cosh(\nu(s)(z-1))}{\sinh(\nu(s))}\right).\end{aligned} \tag{21}$$

[1] We keep the notation of Smith et al. and use the Greek letter "nu" for this variable, but always write it as $\nu(s)$ to distinguish it from cell voltage, which is written as $v(t)$.

This is the first transfer function we have set out to find, and is equivalent to the corresponding result in [8,9] except for the $R_{film}$ term embedded inside of our $\nu(s)$.

The overpotential $\eta$ is given by Eq. (6) and repeated below,

$$\eta = \phi_s - \phi_e - U_{ocp} - jFR_{film}.$$

We use Eq. (11) and the definition of $\phi_{s-e} = \phi_s - \phi_e = \tilde{\phi}_{s-e} + U_{ocp}(c_{s,0})$ to get

$$\phi_{s-e} = FR_{tot}j + U_{ocp}(c_{s,0}) + \left[\left.\frac{\partial U_{ocp}}{\partial c_{s,e}}\right|_{c_{s,0}}\right]\tilde{c}_{s,e},$$

and

$$\eta = FR_{ct}j - U_{ocp}(c_{s,e}) + U_{ocp}(c_{s,0}) + \left[\left.\frac{\partial U_{ocp}}{\partial c_{s,e}}\right|_{c_{s,0}}\right]\tilde{c}_{s,e}.$$

We note that $U_{ocp}(c_{s,e}) \approx U_{ocp}(c_{s,0}) + [(\partial U_{ocp}/\partial c_{s,e})|_{c_{s,0}}]\tilde{c}_{s,e}$, leaving us with the following transfer function for $\eta$,

$$\frac{\eta(z,s)}{I_{app}(s)} = FR_{ct}\frac{J(z,s)}{I_{app}(s)}. \tag{22}$$

Finally, the transfer function for the surface concentration is given by

$$\begin{aligned}\frac{\tilde{C}_{s,e}(z,s)}{I_{app}(s)} &= \frac{\tilde{C}_{s,e}(z,s)}{J(z,s)}\frac{J(z,s)}{I_{app}(s)} \\ &= \frac{\nu(s)R_s}{a_s F L_n A D_s\left(\kappa^{eff}+\sigma^{eff}\right)}\left(\frac{\tanh(\beta)}{\tanh(\beta)-\beta}\right) \\ &\quad\times\left(\frac{\sigma^{eff}\cosh(\nu(s)z)+\kappa^{eff}\cosh(\nu(s)(z-1))}{\sinh(\nu(s))}\right).\end{aligned} \tag{23}$$

Eqs. (21)–(23) are the first three transfer functions used in the reduced-order cell model. These transfer functions are valid for the negative electrode. For the positive electrode, the derivation follows exactly the same steps, and the resulting transfer functions are the same as those for the negative electrode region, but are multiplied by −1, and the negative-electrode parameters are replaced by their corresponding positive-electrode values.

### 2.3. Transfer function for solid potential $\phi_s(z,t)$

We now proceed to derive an independent transfer function for the solid potential $\phi_s(z,t)$ in the negative electrode. From Eq. (14) we have

$$\frac{\sigma^{eff}}{L_n^2}\frac{\partial^2}{\partial z^2}\phi_s = a_s F j.$$

Integrating both sides of the equation from 0 to $z$ and using the boundary condition $-((\sigma^{eff}/L_n)(\partial/\partial z)\phi_s(z,t))|_{z=0} = i_{app}/A$ gives

$$\frac{\partial}{\partial z}\phi_s(z,t) = \frac{-L_n i_{app}}{A\sigma^{eff}} + \frac{L_n^2 a_s F}{\sigma^{eff}}\int_0^z j(\zeta,t)\mathrm{d}\zeta.$$

Taking the Laplace transform and dividing both sides of the equation by $I_{app}(s)$ gives,

$$\frac{\partial}{\partial z}\frac{\Phi_s(z,s)}{I_{app}(s)} = \frac{-L_n}{A\sigma^{eff}} + \frac{L_n^2 a_s F}{\sigma^{eff}}\int_0^z \frac{J(\zeta,s)}{I_{app}(s)}\mathrm{d}\zeta. \tag{24}$$

We define a debiased variable $\tilde{\phi}_s(z,t) = \phi_s(z,t) - \phi_s(0,t)$, and integrate both sides of Eq. (24) to give

$$\frac{\widetilde{\Phi}_s(z,s)}{I_{app}(s)} = -\frac{L_n\kappa^{eff}(\cosh(\nu(s)) - \cosh((z-1)\nu(s)))}{A\sigma^{eff}\left(\kappa^{eff}+\sigma^{eff}\right)\nu(s)\sinh(\nu(s))} - \frac{L_n\sigma^{eff}(1-\cosh(z\nu(s)) + z\nu(s)\sinh(\nu(s)))}{A\sigma^{eff}\left(\kappa^{eff}+\sigma^{eff}\right)\nu(s)\sinh(\nu(s))}. \quad (25)$$

As before, the positive-electrode version of this transfer function is simply multiplied by −1, and negative-electrode parameters are replaced by their corresponding positive-electrode values.

### 2.4. Transfer function for electrolyte potential $\phi_e(x,t)$

We now develop an independent transfer function for $\phi_e$ as a function of $x$, the non-normalized length. Since we are dealing with variables that exist over the entire cell width and not over a single electrode only, we also introduce subscripts "$n$" to denote parameter values corresponding to the negative electrode, "$m$" to denote values in the separator region, and "$p$" to denote values in the positive electrode, whenever making a distinction is necessary.[2] Starting with Eq. (4), and integrating once with respect to $x$ gives

$$\frac{\partial\phi_e(x,t)}{\partial x} = \frac{-i_e(x,t)}{\kappa^{eff}} + \frac{2RT}{F}\left(1-t_+^0\right)\frac{\partial \ln c_e(x,t)}{\partial x}, \quad (26)$$

where

$$i_e(x,t) = \begin{cases} \int_0^x a_s F j(\xi,t)\,d\xi, & 0 \le x \le L_n; \\ i_{app}(t)/A, & L_n \le x \le L_n + L_m; \\ \frac{i_{app}(t)}{A} - \int_{L_n+L_m}^x a_s F j(\xi,t)\,d\xi, & L_n + L_m \le x \le L. \end{cases}$$

In the rigorous electrode model, the effective ionic conductivity, $\kappa^{eff}$, is a function of $c_e$. For the reduced-order model, $\kappa^{eff}$ is constant and determined from the equilibrium $c_e$ value. The transfer function for the ionic current is found by integrating the previously derived equation for the reaction flux transfer function. In the negative electrode this is

$$\frac{I_e(x,s)}{I_{app}(s)} = a_s F\int_0^x \frac{J(\xi,s)}{I_{app}(s)}\,d\xi = \frac{\sigma^{eff}\sinh\left(\frac{x\nu(s)}{L_n}\right) - \kappa^{eff}\sinh\left(\frac{(L_n-x)\nu(s)}{L_n}\right)}{A\left(\kappa^{eff}+\sigma^{eff}\right)\sinh(\nu(s))} + \frac{\kappa^{eff}}{A\left(\kappa^{eff}+\sigma^{eff}\right)}.$$

The transfer function for $i_e(x,t)$ in the separator is $I_e(x,s)/I_{app}(s) = 1/A$. The transfer function for the positive electrode is

$$\frac{I_e(x,s)}{I_{app}(s)} = \frac{1}{A} - a_s F\int_0^x \frac{J(\xi,s)}{I_{app}(s)}\,d\xi = \frac{\sigma^{eff}\sinh\left(\frac{(L-x)\nu(s)}{L_p}\right) + \kappa^{eff}\sinh\left(\frac{(L_n+L_m-x)\nu(s)}{L_p}\right)}{A\left(\kappa^{eff}+\sigma^{eff}\right)\sinh(\nu(s))} + \frac{\kappa^{eff}}{A\left(\kappa^{eff}+\sigma^{eff}\right)}.$$

[2] The subscript "m" is used to denote the electrolyte phase in the separator in the "middle" of the cell, as "s" is already used to denote the solid phase.

In order to solve the PDE for $\phi_e$ we integrate Eq. (26) to arrive at

$$\phi_e(x,t) - \phi_e(0,t) = \int_0^x \left(\frac{-i_e(\xi,t)}{\kappa^{eff}} + \frac{2RT}{F}\left(1-t_+^0\right)\frac{\partial \ln c_e(\xi,t)}{\partial\xi}\right)d\xi. \quad (27)$$

We define $\tilde{\phi}_e(x,t) = \phi_e(x,t) - \phi_e(0,t)$. $\tilde{\phi}_e(x,t)$ is comprised of two parts corresponding to the two parts of the equation above:

$$\left[\tilde{\phi}_e(x,t)\right]_1 = \int_0^x \frac{-i_e(\xi,t)}{\kappa^{eff}}d\xi$$

$$\left[\tilde{\phi}_e(x,t)\right]_2 = \int_0^x \frac{2RT}{F}\left(1-t_+^0\right)\frac{\partial \ln c_e(\xi,t)}{\partial\xi}d\xi.$$

The first part $[\tilde{\phi}_e(x,t)]_1$ is solved using transfer functions. The second part, $[\tilde{\phi}_e(x,t)]_2$ will be determined from the value of $c_e(x,t)$, which we find in Section 2.5. The transfer function for the first part, for locations $x$ in the negative electrode, is

$$\frac{\left[\widetilde{\Phi}_e(x,s)\right]_1}{I_{app}(s)} = \frac{-1}{\kappa_n^{eff}}\int_0^x \frac{I_e(\xi,s)}{I_{app}(s)}d\xi = \frac{L_n\left(\frac{\sigma_n^{eff}}{\kappa_n^{eff}}\right)\left(1-\cosh\left(\frac{x\nu_n(s)}{L_n}\right)\right) - x\nu_n(s)\sinh(\nu_n(s))}{A\left(\kappa_n^{eff}+\sigma_n^{eff}\right)\nu_n(s)\sinh(\nu_n(s))} + \frac{L_n\left(\cosh(\nu_n(s)) - \cosh\left(\frac{(L_n-x)\nu_n(s)}{L_n}\right)\right)}{A\left(\kappa_n^{eff}+\sigma_n^{eff}\right)\nu_n(s)\sinh(\nu_n(s))}. \quad (28)$$

For locations $x$ in the separator region, the transfer function is

$$\frac{\left[\widetilde{\Phi}_e(x,s)\right]_1}{I_{app}(s)} = \frac{L_n - x}{A\kappa_m^{eff}} + \frac{L_n\left(\left(1-\frac{\sigma_n^{eff}}{\kappa_n^{eff}}\right)\tanh\left(\frac{\nu_n(s)}{2}\right) - \nu_n(s)\right)}{A\left(\kappa_n^{eff}+\sigma_n^{eff}\right)\nu_n(s)}. \quad (29)$$

Finally, for locations $x$ in the positive electrode, the transfer function is

$$\frac{\left[\widetilde{\Phi}_e(x,s)\right]_1}{I_{app}(s)} = \frac{-L_m}{A\kappa_m^{eff}} + \frac{L_n\left(\left(1-\frac{\sigma_n^{eff}}{\kappa_n^{eff}}\right)\tanh\left(\frac{\nu_n(s)}{2}\right) - \nu_n(s)\right)}{A\left(\kappa_n^{eff}+\sigma_n^{eff}\right)\nu_n(s)} - \frac{L_p\left(1+\frac{\sigma_p^{eff}}{\kappa_p^{eff}}\cosh(\nu_p(s))\right)}{A\left(\kappa_p^{eff}+\sigma_p^{eff}\right)\sinh(\nu_p(s))\nu_p(s)} + \frac{L_p\cosh\left(\frac{(L_n+L_m-x)\nu_p(s)}{L_p}\right)}{A\left(\kappa_p^{eff}+\sigma_p^{eff}\right)\sinh(\nu_p(s))\nu_p(s)} + \frac{L_p\left(\frac{\sigma_p^{eff}}{\kappa_p^{eff}}\cosh\left(\frac{(L-x)\nu_p(s)}{L_p}\right)\right)}{A\left(\kappa_p^{eff}+\sigma_p^{eff}\right)\sinh(\nu_p(s))\nu_p(s)} + \frac{(L_n+L_m-x)}{A\left(\kappa_p^{eff}+\sigma_p^{eff}\right)}. \quad (30)$$

For the second term of Eq. (27) we have

$$\left[\tilde{\phi}_e(x,t)\right]_2 = \frac{2RT(1-t_+^0)}{F}\int_0^x \frac{\partial \ln c_e(\xi,t)}{\partial \xi}d\xi = \frac{2RT(1-t_+^0)}{F}\ln\left(\frac{c_e(x,t)}{c_e(0,t)}\right). \quad (31)$$

In our final reduced-order model, we will be interested in values of the electrolyte potential at particular locations across the cell. At each $x$ location, we will then have a transfer function to solve for $[\tilde{\Phi}_e(x,s)]_1$. This transfer function will be from Eq. (28), Eq. (29) or Eq. (30) depending on whether $x$ is in the negative electrode, separator, or positive electrode, respectively. In the next section, we derive an analytic transfer function for the electrolyte concentration $c_e(x,t)$, which we need to be able to compute $[\tilde{\phi}_e(x,t)]_2$.

### 2.5. Transfer function for the electrolyte concentration $c_e(x,t)$

In [8,9], Smith et al. used transfer functions to solve for $j$, $\phi_{s-e}$, $\eta$, and $c_{s,e}$, but then used the finite-element method to solve for $c_e$. We prefer to use the transfer function approach for all variables, since this lets us jointly optimize the reduced-order model over all transfer functions using the DRA. So, in this section, we focus on deriving a transfer function for $c_e(x,t)$.

The governing equation for the electrolyte concentration is given by Eq. (2), repeated here but now explicitly noting the $x$-dependence of $\varepsilon_e$ and $D_e^{\text{eff}}$,

$$\varepsilon_e(x)\frac{\partial c_e(x,t)}{\partial t} = \frac{\partial}{\partial x}\left(D_e^{\text{eff}}(x)\frac{\partial}{\partial x}c_e(x,t)\right) + \left(1-t_+^0\right)a_s j(x,t), \quad (32)$$

with boundary conditions

$$\frac{\partial c_e(0,t)}{\partial x} = 0 \quad \text{and} \quad \frac{\partial c_e(L,t)}{\partial x} = 0,$$

and uniform initial condition $c_e(x,0) = c_{e,0}$.

The analytic transfer function for the electrolyte concentration is derived using the following steps. First, we find the homogeneous solution to Eq. (32) using the method of separation of variables and by finding eigenfunctions that are orthonormal with respect to the weighting function $\varepsilon_e(x)$. The solution to the inhomogeneous problem is found by projecting the concentration function onto these eigenfunctions to find the generalized Fourier coefficients. Finally, we derive the Laplace domain transfer function that will solve for the Fourier coefficients.

#### 2.5.1. Solution to the homogeneous problem

We first use the method of separation of variables to find the solution to the homogeneous problem. Our approach is similar to [12] but whereas Schmidt et al. required $D_e^{\text{eff}}$ and $\varepsilon_e$ to be constant across the entire cell, we allow for different values in each of the three regions of the cell. In order to simplify notation, we use

$$\varepsilon_e(x) = \begin{cases} \varepsilon_n, & x < L_n; \\ \varepsilon_m, & L_n \le x < L_n + L_m; \\ \varepsilon_p, & L_n + L_m \le x < L. \end{cases}$$

The values of $\varepsilon_n$, $\varepsilon_m$, and $\varepsilon_p$ are constant. Likewise, the electrolyte diffusivity is assumed to be constant within each region and we simplify the notation using

$$D_e^{\text{eff}}(x) = \begin{cases} D_n, & x < L_n; \\ D_m, & L_n \le x < L_n + L_m; \\ D_p, & L_n + L_m \le x < L. \end{cases}$$

The homogeneous problem is written as

$$\frac{\partial c_e(x,t)}{\partial t} = \frac{1}{\varepsilon_e(x)}\frac{\partial}{\partial x}\left(D_e^{\text{eff}}(x)\frac{\partial c_e(x,t)}{\partial x}\right). \quad (33)$$

In addition to the boundary conditions given above we have internal boundary conditions where the three regions of the cell join. These internal boundary conditions are

$$c_e\left(L_n^-,t\right) = c_e\left(L_n^+,t\right)$$
$$c_e\left((L_n+L_m)^-,t\right) = c_e\left((L_n+L_m)^+,t\right)$$
$$D_n\frac{\partial c_e\left(L_n^-,t\right)}{\partial x} = D_m\frac{\partial c_e\left(L_n^+,t\right)}{\partial x}$$
$$D_m\frac{\partial c_e\left((L_n+L_m)^-,t\right)}{\partial x} = D_p\frac{\partial c_e\left((L_n+L_m)^+,t\right)}{\partial x}.$$

Using the method of separation of variables, the solution to Eq. (33) can be split into a function of time only and a function of position only

$$c_e(x,t) = h(t)\Psi(x).$$

Substituting this assumed form into Eq. (33) gives

$$\frac{dh(t)}{dt}\Psi(x) = \frac{1}{\varepsilon_e(x)}\frac{\partial}{\partial x}D_e^{\text{eff}}(x)h(t)\frac{d\Psi(x)}{dx}.$$

Separating the time-dependent variables on one side of the equation, the position dependent variables on the other, we get

$$\frac{1}{h(t)}\frac{dh(t)}{dt} = \frac{1}{\varepsilon_e(x)\Psi(x)}\frac{d}{dx}\left(D_e^{\text{eff}}(x)\frac{d\Psi(x)}{dx}\right).$$

Since one side of the equation is a function of time only, and the other side is a function of position only, and the equations are equal to each other for all values of $t$ and $x$, then both sides must be constant:

$$\frac{1}{h(t)}\frac{dh(t)}{dt} = \frac{1}{\varepsilon_e(x)\Psi(x)}\frac{d}{dx}\left(D_e^{\text{eff}}(x)\frac{d\Psi(x)}{dx}\right) = -\lambda.$$

Splitting this into separate equations in time and position gives

$$\frac{dh(t)}{dt} = -\lambda h(t) \quad (34)$$

$$\frac{d}{dx}\left(D_e^{\text{eff}}(x)\frac{d\Psi(x)}{dx}\right) = -\lambda\varepsilon_e(x)\Psi(x). \quad (35)$$

There are infinitely many specific eigenvalues $\lambda$ that satisfy these equations, with specific corresponding eigenfunctions $\Psi$. We change notation so that $h(t) \mapsto h(t;\lambda)$ and change $\Psi(x) \mapsto \Psi(x;\lambda)$. The solution to Eq. (34) is then of the form

$$h(t;\lambda) = h(0;\lambda)e^{-\lambda t}.$$

Eigenfunction solutions to Eq. (35) have three distinct parts: one each for the negative electrode, the separator, and the positive electrode. For the negative electrode, we have

$$\Psi_{\mathrm{n}}(x;\lambda) = k_1\cos\left(\sqrt{\lambda\varepsilon_{\mathrm{n}}/D_{\mathrm{n}}}x\right) + k_2\sin\left(\sqrt{\lambda\varepsilon_{\mathrm{n}}/D_{\mathrm{n}}}x\right).$$

The boundary condition at $x = 0$ eliminates the sine term, which leaves

$$\Psi_{\mathrm{n}}(x;\lambda) = k_1\cos\left(\sqrt{\frac{\lambda\varepsilon_{\mathrm{n}}}{D_{\mathrm{n}}}}x\right).$$

In the separator and positive electrode, the eigenfunctions are

$$\Psi_{\mathrm{m}}(x;\lambda) = k_3\cos\left(\sqrt{\frac{\lambda\varepsilon_{\mathrm{m}}}{D_{\mathrm{m}}}}x\right) + k_4\sin\left(\sqrt{\frac{\lambda\varepsilon_{\mathrm{m}}}{D_{\mathrm{m}}}}x\right)$$
$$\Psi_{\mathrm{p}}(x;\lambda) = k_5\cos\left(\sqrt{\frac{\lambda\varepsilon_{\mathrm{p}}}{D_{\mathrm{p}}}}x\right) + k_6\sin\left(\sqrt{\frac{\lambda\varepsilon_{\mathrm{p}}}{D_{\mathrm{p}}}}x\right).$$

Using the internal boundary conditions, we can solve for $k_3$ and $k_4$ in terms of $k_1$ by solving the linear equations

$$\begin{bmatrix} \cos\left(\sqrt{\frac{\lambda\varepsilon_{\mathrm{m}}}{D_{\mathrm{m}}}}L_{\mathrm{n}}\right) & \sin\left(\sqrt{\frac{\lambda\varepsilon_{\mathrm{m}}}{D_{\mathrm{m}}}}L_{\mathrm{n}}\right) \\ -\sqrt{\lambda\varepsilon_{\mathrm{m}}D_{\mathrm{m}}}\sin\left(\sqrt{\frac{\lambda\varepsilon_{\mathrm{m}}}{D_{\mathrm{m}}}}L_{\mathrm{n}}\right) & \sqrt{\lambda\varepsilon_{\mathrm{m}}D_{\mathrm{m}}}\cos\left(\sqrt{\frac{\lambda\varepsilon_{\mathrm{m}}}{D_{\mathrm{m}}}}L_{\mathrm{n}}\right) \end{bmatrix}\begin{bmatrix} k_3 \\ k_4 \end{bmatrix}$$
$$= k_1\begin{bmatrix} \cos\left(\sqrt{\frac{\lambda\varepsilon_{\mathrm{n}}}{D_{\mathrm{n}}}}L_{\mathrm{n}}\right) \\ -\sqrt{\lambda\varepsilon_{\mathrm{n}}D_{\mathrm{n}}}\sin\left(\sqrt{\frac{\lambda\varepsilon_{\mathrm{n}}}{D_{\mathrm{n}}}}L_{\mathrm{n}}\right) \end{bmatrix}.$$

In a similar manner, we solve for $k_5$ and $k_6$ in terms of $k_3$ and $k_4$ where $x^* = L_{\mathrm{n}} + L_{\mathrm{m}}$:

$$\begin{bmatrix} \cos\left(\sqrt{\frac{\lambda\varepsilon_{\mathrm{p}}}{D_{\mathrm{p}}}}x^*\right) & \sin\left(\sqrt{\frac{\lambda\varepsilon_{\mathrm{p}}}{D_{\mathrm{p}}}}x^*\right) \\ -\sqrt{\lambda\varepsilon_{\mathrm{p}}D_{\mathrm{p}}}\sin\left(\sqrt{\frac{\lambda\varepsilon_{\mathrm{p}}}{D_{\mathrm{p}}}}x^*\right) & \sqrt{\lambda\varepsilon_{\mathrm{p}}D_{\mathrm{p}}}\cos\left(\sqrt{\frac{\lambda\varepsilon_{\mathrm{p}}}{D_{\mathrm{p}}}}x^*\right) \end{bmatrix}\begin{bmatrix} k_5 \\ k_6 \end{bmatrix}$$
$$= \begin{bmatrix} \cos\left(\sqrt{\frac{\lambda\varepsilon_{\mathrm{m}}}{D_{\mathrm{m}}}}x^*\right) & \sin\left(\sqrt{\frac{\lambda\varepsilon_{\mathrm{m}}}{D_{\mathrm{m}}}}x^*\right) \\ -\sqrt{\lambda\varepsilon_{\mathrm{m}}D_{\mathrm{m}}}\sin\left(\sqrt{\frac{\lambda\varepsilon_{\mathrm{m}}}{D_{\mathrm{m}}}}x^*\right) & \sqrt{\lambda\varepsilon_{\mathrm{m}}D_{\mathrm{m}}}\cos\left(\sqrt{\frac{\lambda\varepsilon_{\mathrm{m}}}{D_{m}}}x^*\right) \end{bmatrix}\begin{bmatrix} k_3 \\ k_4 \end{bmatrix}.$$

The eigenfunction over the entire cell cell is then

$$\Psi(x;\lambda) = \begin{cases} \Psi_{\mathrm{n}}(x;\lambda), & 0 \le x < L_{\mathrm{n}}; \\ \Psi_{\mathrm{m}}(x;\lambda), & L_{\mathrm{n}} \le x < L_{\mathrm{n}} + L_{\mathrm{m}}; \\ \Psi_{\mathrm{p}}(x;\lambda), & L_{\mathrm{n}} + L_{\mathrm{m}} \le x \le L. \end{cases} \quad (36)$$

By Sturm–Liouville theory [13], the different eigenfunctions are automatically orthogonal with respect to the weighting function $\varepsilon_{\mathrm{e}}(x)$, and $k_1$ is chosen to satisfy

$$\int_0^L \Psi^2(x;\lambda)\varepsilon_{\mathrm{e}}(x)\mathrm{d}x = 1,$$

making them furthermore orthonormal with respect to $\varepsilon_{\mathrm{e}}(x)$. The final boundary condition $\partial\Psi(L;\lambda)/\partial x = 0$ allows us to find the set of $\lambda$ which solve the homogeneous PDE. We denote specific solutions as $\lambda_k$, and search for solutions as roots of

$$\frac{\mathrm{d}\Psi(L;\lambda_{\mathrm{k}})}{\mathrm{d}x} = -k_5\sin\left(\sqrt{\frac{\lambda_{\mathrm{k}}\varepsilon_{\mathrm{p}}}{D_{\mathrm{p}}}}L\right) + k_6\cos\left(\sqrt{\frac{\lambda_{\mathrm{k}}\varepsilon_{\mathrm{p}}}{D_{\mathrm{p}}}}L\right) = 0. \quad (37)$$

It is not possible to find a closed-form solution for $\lambda_{\mathrm{k}}$ as $k_5$ and $k_6$ are themselves functions of $\lambda_{\mathrm{k}}$. Instead, we do a numerical search of the zero crossings of Eq. (37) until we find for the desired number of eigenvalues.[3] We denote the ordered set of eigenvalues as $\{\lambda_{\mathrm{k}}\}$. Then, the solution to the homogeneous problem is the superposition

$$c_{\mathrm{e}}(x,t) = \sum_{k=0}^{\infty} h(0;\lambda_{\mathrm{k}})\Psi(x;\lambda_{\mathrm{k}})e^{-\lambda_{\mathrm{k}}t}.$$

*2.5.2. Solution to the inhomogeneous problem*

We now generalize the homogeneous solution to the inhomogeneous case to solve

$$\frac{\partial c_{\mathrm{e}}(x,t)}{\partial t} = \frac{1}{\varepsilon_{\mathrm{e}}(x)}\frac{\partial}{\partial x}\left(D_{\mathrm{e}}^{\mathrm{eff}}(x)\frac{\partial c_{\mathrm{e}}(x,t)}{\partial x}\right) + \frac{a_{\mathrm{s}}(1-t_+^0)}{\varepsilon_{\mathrm{e}}(x)}j(x,t). \quad (38)$$

We transform $c_e(x,t)$ into a series expansion using the eigenfunctions from the previous section as a basis set

$$c_{\mathrm{e}}(x,t) = \sum_{k=0}^{\infty} c_{\mathrm{e,k}}^*(t)\Psi(x;\lambda_{\mathrm{k}}), \quad (39)$$

where $c_{\mathrm{e,k}}^*(t)$ are the generalized Fourier coefficients of $c_{\mathrm{e}}(x,t)$. Taking the partial derivative of this equation with respect to time gives

$$\frac{\partial c_{\mathrm{e}}(x,t)}{\partial t} = \sum_{k=0}^{\infty}\frac{\mathrm{d}c_{\mathrm{e,k}}^*(t)}{\mathrm{d}t}\Psi(x;\lambda_{\mathrm{k}}). \quad (40)$$

Substituting Eq. (40) into Eq. (38) gives

$$\sum_{k=0}^{\infty}\frac{\mathrm{d}c_{\mathrm{e,k}}^*(t)}{\mathrm{d}t}\Psi(x;\lambda_{\mathrm{k}}) = \frac{1}{\varepsilon_{\mathrm{e}}(x)}\frac{\partial}{\partial x}\left(D_{\mathrm{e}}^{\mathrm{eff}}(x)\frac{\partial}{\partial x}c_{\mathrm{e}}(x,t)\right) + \frac{a_{\mathrm{s}}(1-t_+^0)}{\varepsilon_{\mathrm{e}}(x)}j(x,t).$$

To reduce the left-hand side of the above equation, we can multiply both sides by $\Psi(x;\lambda_{\mathrm{m}})\varepsilon_{\mathrm{e}}(x)$ and integrate from 0 to $L$.

$$\int_0^L\sum_{k=0}^{\infty}\frac{\mathrm{d}c_{\mathrm{e,k}}^*(t)}{\mathrm{d}t}\Psi(x;\lambda_{\mathrm{k}})\Psi(x;\lambda_{\mathrm{m}})\varepsilon_{\mathrm{e}}(x)\mathrm{d}x$$
$$= \int_0^L\Psi(x;\lambda_{\mathrm{m}})\frac{\partial}{\partial x}\left(D_{\mathrm{e}}^{\mathrm{eff}}(x)\frac{\partial c_{\mathrm{e}}(x,t)}{\partial x}\right)\mathrm{d}x$$
$$+\int_0^L a_{\mathrm{s}}\left(1-t_+^0\right)j(x,t)\Psi(x;\lambda_{\mathrm{m}})\mathrm{d}x.$$

[3] Note that one aspect of Sturm–Liouville theory guarantees that the $k$th eigenfunction $\Psi(x;\lambda_{\mathrm{k}})$ has $k$ zero crossings in (0,L), so by plotting the eigenfunctions over the cell width it is simple to detect if the numeric search has succeeded (cf. Fig. 4 for an example of what the eigenfunctions can look like). In practice, we find that relatively few—between about five and ten—eigenvalue/eigenfunction pairs are needed to approximate $c_{\mathrm{e}}$ very well.

The eigenfunctions are orthonormal with respect to $\varepsilon_e(x)$, so the integral on the left-hand side is non-zero only when $m = n$. This gives

$$\frac{dc^*_{e,k}(t)}{dt} = \int_0^L \Psi(x;\lambda_k)\frac{\partial}{\partial x}\left(D_e^{eff}(x)\frac{\partial c_e(x,t)}{\partial x}\right)dx + \int_0^L a_s\left(1-t_+^0\right)j(x,t)\Psi(x;\lambda_k)dx. \quad (41)$$

Using Green's identity [13] on the first term on the right-hand side of the equation gives,

$$\int_0^L\left[c_e(x,t)\frac{\partial}{\partial x}\left(D_e^{eff}(x)\frac{\partial\Psi(x;\lambda_k)}{\partial x}\right)-\Psi(x;\lambda_k)\frac{\partial}{\partial x}\left(D_e^{eff}(x)\frac{\partial c_e(x,t)}{\partial x}\right)\right]dx = D_e^{eff}(x)\left(c_e(x,t)\frac{\partial\Psi(x;\lambda_k)}{\partial x}-\Psi(x;\lambda_k)\frac{\partial c_e(x,t)}{\partial x}\right)\Big|_0^L. \quad (42)$$

The right-hand side goes to zero because of the boundary conditions

$$\left.\frac{\partial\Psi(x;\lambda_k)}{\partial x}\right|_{x\in\{0,L\}} = \left.\frac{\partial c_e(x,t)}{\partial x}\right|_{x\in\{0,L\}} = 0.$$

The left-hand side of Eq. (42) has two parts. The first part can be written as

$$\int_0^L c_e(x,t)\frac{\partial}{\partial x}\left(D_e^{eff}(x)\frac{\partial\Psi(x;\lambda_k)}{\partial x}\right)dx = -\lambda_k\int_0^L c_e(x,t)\Psi(x;\lambda_k)\varepsilon_e(x)dx, \quad (43)$$

because $\Psi(x;\lambda_k)$ satisfies the homogeneous case Eq. (35)

$$\frac{\partial}{\partial x}\left(D_e^{eff}(x)\frac{\partial\Psi(x;\lambda_k)}{\partial x}\right)+\lambda_k\varepsilon_e(x)\Psi(x;\lambda_k) = 0.$$

Since the right-hand side of Eq. (42) is zero, we can write

$$\int_0^L \Psi(x;\lambda_k)\frac{\partial}{\partial x}\left(D_e^{eff}(x)\frac{\partial c_e(x,t)}{\partial x}\right)dx = -\lambda_k\int_0^L c_e(x,t)\varepsilon_e(x)\Psi(x;\lambda_k)dx.$$

Using this in Eq. (41) gives

$$\begin{aligned}\frac{dc^*_{e,k}(t)}{dt} &= -\lambda_k\int_0^L c_e(x,t)\Psi(x;\lambda_k)\varepsilon_e(x)dx + \int_0^L a_s\left(1-t_+^0\right)j(x,t)\Psi(x;\lambda_k)dx\\ &= -\lambda_k c^*_{e,k}(t) + \int_0^L a_s\left(1-t_+^0\right)j(x,t)\Psi(x;\lambda_k)dx\\ &= -\lambda_k c^*_{e,k}(t) + j^*_k(t;\lambda_k),\end{aligned}$$

where we have defined

$$j^*_k(t;\lambda_k) = \int_0^L a_s\left(1-t_+^0\right)j(x,t)\Psi(x;\lambda_k)dx.$$

*2.5.3. Transfer function*

To compute $c_e(x,t)$ via transfer-function methods, we note that $c_e(x,t)$ is formed from a summation of $c^*_{e,k}(t)$ terms. We can compute $c_e(x,t)$ if we know $c^*_{e,k}(t)$, so we proceed by finding a transfer function for $c^*_{e,k}(t)$:

$$\begin{aligned}\frac{dc^*_{e,k}(t)}{dt} &= -\lambda_k c^*_{e,k}(t) + j^*_k(t)\\ sC^*_{e,k}(s) &= -\lambda_k C^*_{e,k}(s) + J^*_k(s)\\ \frac{C^*_{e,k}(s)}{I_{app}(s)} &= \frac{1}{s+\lambda_k}\frac{J^*_k(s)}{I_{app}(s)}.\end{aligned}$$

We further examine $j^*_k(t)$,

$$\begin{aligned}j^*_k(t) &= \int_0^L a_s\left(1-t_+^0\right)j(x,t)\Psi(x;\lambda_k)dx\\ &= \int_0^{L_n} a_s\left(1-t_+^0\right)j(x,t)\Psi(x;\lambda_k)dx\\ &\quad + \int_{L_n+L_m}^{L} a_s\left(1-t_+^0\right)j(x,t)\Psi(x;\lambda_k)dx\\ &= j_k^{neg^*}(t) + j_k^{pos^*}(t).\end{aligned}$$

For the negative electrode,

$$\begin{aligned}j_k^{neg^*}(t) &= a_s(1-t_+^0)\int_0^{L_n} j(x,t)\Psi(x;\lambda_k)dx\\ \frac{J_k^{neg^*}(s)}{I_{app}(s)} &= a_s\left(1-t_+^0\right)\int_0^{L_n}\frac{J(x/L_n,s)}{I_{app}(s)}\Psi(x;\lambda_k)dx.\end{aligned} \quad (44)$$

Note that $J(z,s)/I_{app}(s)$ is given by Eq. (21), where $z = x/L_n$ in the negative electrode. Performing the integration of Eq. (44) gives,

$$\frac{J_k^{neg^*}(s)}{I_{app}(s)} = \frac{k_1(1-t_+^0)L_n^*\sin\left(L_n^*\right)\left(\kappa_n^{eff}+\sigma_n^{eff}\cosh(\nu_n(s))\right)\nu_n(s)}{AF\left(\kappa_n^{eff}+\sigma_n^{eff}\right)\left(\left(L_n^*\right)^2+\nu_n^2(s)\right)\sinh(\nu_n(s))} + \frac{k_1(1-t_+^0)\left(\kappa_n^{eff}+\sigma_n^{eff}\cos\left(L_n^*\right)\right)\nu_n^2(s)}{AF\left(\kappa_n^{eff}+\sigma_n^{eff}\right)\left(\left(L_n^*\right)^2+\nu_n^2(s)\right)}, \quad (45)$$

where $L_n^* = L_n\sqrt{\varepsilon_n\lambda_k/D_n}$. For the positive electrode,

$$j_k^{pos^*}(t) = a_s(1-t_+^0)\int_{L_n+L_m}^{L} j(x,t)\Psi(x;\lambda_k)dx$$

$$\frac{J_k^{pos^*}(s)}{I_{app}(s)} = a_s\left(1-t_+^0\right)\int_{L_n+L_m}^{L}\frac{J((L-x)/L_p,s)}{I_{app}(s)}\Psi(x;\lambda_k)dx,$$

which gives,

$$\begin{aligned}\frac{J_k^{pos^*}(s)}{I_{app}(s)} =& \frac{k_6(1-t_+^0)L_p^*\cos(L^*)\left(\sigma_p^{eff}+\kappa_p^{eff}\cosh(\nu_p(s))\right)\nu_p(s)}{AF\left(\kappa_p^{eff}+\sigma_p^{eff}\right)\left(\left(L_p^*\right)^2+\nu_p^2(s)\right)\sinh(\nu_p(s))}\\ &-\frac{k_5(1-t_+^0)L_p^*\sin\left(L_p^*\right)\left(\kappa_p^{eff}+\sigma_p^{eff}\cosh(\nu_p(s))\right)\nu_p(s)}{AF\left(\kappa_p^{eff}+\sigma_p^{eff}\right)\left(\left(L_p^*\right)^2+\nu_p^2(s)\right)\sinh(\nu_p(s))}\\ &+\frac{k_6(1-t_+^0)L_p^*\cos\left(L_{nm}^*\right)\left(\kappa_p^{eff}+\sigma_p^{eff}\cosh(\nu_p(s))\right)\nu_p(s)}{AF\left(\kappa_p^{eff}+\sigma_p^{eff}\right)\left(\left(L_p^*\right)^2+\nu_p^2(s)\right)\sinh(\nu_p(s))}\\ &-\frac{k_5(1-t_+^0)L_p^*\left(\sin(L^*)\left(\sigma_p^{eff}+\kappa_p^{eff}\cosh(\nu_p(s))\right)\right)\nu_p(s)}{AF\left(\kappa_p^{eff}+\sigma_p^{eff}\right)\left(\left(L_p^*\right)^2+\nu_p^2(s)\right)\sinh(\nu_p(s))}\\ &-\frac{k_5(1-t_+^0)\left(\sigma_p^{eff}\cos\left(L_{nm}^*\right)+\kappa_p^{eff}\cos(L^*)\right)\nu_p^2(s)}{AF\left(\kappa_p^{eff}+\sigma_p^{eff}\right)\left(\left(L_p^*\right)^2+\nu_p^2(s)\right)}\\ &-\frac{k_6(1-t_+^0)\left(\sigma_p^{eff}\sin(L_{nm}^*)+\kappa_p^{eff}\sin(L^*)\right)\nu_p^2(s)}{AF\left(\kappa_p^{eff}+\sigma_p^{eff}\right)\left(\left(L_p^*\right)^2+\nu_p^2(s)\right)},\end{aligned} \tag{46}$$

where $L_p^* = L_p\sqrt{\varepsilon_p\lambda_k/D_p}$, $L_{nm}^* = (L_n+L_m)\sqrt{\varepsilon_p\lambda_k/D_p}$, and $L^* = L\sqrt{\varepsilon_p\lambda_k/D_p}$. The transfer function for the generalized Fourier coefficients of the electrolyte concentration is

$$\frac{C_{e,k}^*(s)}{I_{app}(s)} = \frac{1}{s+\lambda_k}\left[\frac{J_k^{neg^*}(s)}{I_{app}(s)}+\frac{J_k^{pos^*}(s)}{I_{app}(s)}\right]. \tag{47}$$

Since the concentration is given by Eq. (39) we can find a transfer function for $c_e$ at any $x$ location across the cell. This transfer function is given by

$$\frac{C_e(x,s)}{I_{app}(s)} = \sum_{k=0}^{K}\frac{C_{e,k}^*(s)}{I_{app}(s)}\Psi(x;\lambda_k), \tag{48}$$

where $K$ is the number of eigenvalue/eigenfunction expansion terms chosen to approximate the exact solution. The first term in the summation, $(C_{e,0}^*(s)/I_{app(s)})\Psi(x;\lambda_k)$, is equal to the steady-state concentration of lithium in the electrolyte phase, $c_{e,0}$. We define $\tilde{c}_e(x,t) = c_e(x,t) - c_{e,0}$ and remove this term from the summation to give

$$\frac{\tilde{C}_e(x,s)}{I_{app}(s)} = \sum_{k=1}^{K}\frac{C_{e,k}^*(s)}{I_{app}(s)}\Psi(x;\lambda_k). \tag{49}$$

### 2.6. Summary of transfer functions forming the model

Before proceeding, we quickly summarize the transfer functions of the model. Recall that $z$ is a normalized unitless spatial variable in the electrodes that takes on value 0 at the current collectors and 1 at the electrode/separator interface, and that $x$ is the spatial variable across the cell and takes on value 0 at the negative electrode current collector and $L$ at the positive electrode current collector. Common to all of the transfer functions is Eq. (19), which gives the dimensionless function $\nu(s)$ in terms of $\beta = R_s\sqrt{s/D_s}$.

The following transfer functions model cell parameters at any desired sets of spatial locations in the cell based only on the cell input current $I_{app}(s)$.

**Reaction flux:** The local reaction flux transfer function $J(z,s)/I_{app}(s)$ in the negative electrode is given by Eq. (21). In the positive electrode, simply multiply this transfer function by −1, and replace negative-electrode parameters in the equation by the corresponding positive-electrode quantities.

**Overpotential:** The local overpotential transfer function $\eta(z,s)/I_{app}(s)$ in the negative electrode is given by Eq. (22). In the positive electrode, simply multiply this transfer function by −1, and replace negative-electrode parameters in the equation by the corresponding positive-electrode quantities.

**Solid surface concentration:** Lithium concentration in the solid is denoted as $c_s(r,z,t)$. We are concerned here only with the concentration of lithium at the surface of the particles, as that is what determines reaction rate. The surface concentration is denoted as $c_{s,e}(z,t)$. Furthermore, we define a debiased surface concentration that subtracts out the equilibrium concentration: $\tilde{c}_{s,e}(z,t) = c_{s,e}(z,t) - c_{s,0}$. The transfer function of the debiased surface concentration $\tilde{C}_{s,e}(z,s)/I_{app}(s)$ in the negative electrode is given by Eq. (23). In the positive electrode, simply multiply this transfer function by −1, and replace negative-electrode parameters in the equation by the corresponding positive-electrode quantities. And, once the debiased surface concentration is computed, the true surface concentration can be found as $c_{s,e}(z,t) = \tilde{c}_{s,e}(z,t) + c_{s,0}$.

**Potential in solid:** Solid potential in an electrode is denoted as $\phi_s(z,t)$. We define a debiased solid potential that subtracts out the potential at the electrode's current collector where $z = 0$: $\tilde{\phi}_s(z,t) = \phi_s(z,t) - \phi_s(0,t)$. The transfer function $\tilde{\Phi}_s(z,s)/I_{app}(s)$ of the debiased solid potential in the negative electrode is given by Eq. (25). In the positive electrode, simply multiply this transfer function by −1, and replace negative-electrode parameters in the equation by the corresponding positive-electrode quantities. And, since we define the potential of the negative-electrode current collector to be zero, we have $\phi_s(z,t) = \tilde{\phi}_s(z,t)$ in the negative electrode. In the positive electrode, we have that $\phi_s(z,t) = \tilde{\phi}_s(z,t) + \nu(t)$, where $\nu(t)$ is the cell voltage and can be found as described in Section 4.2.

**Potential in electrolyte:** Electrolyte potential is denoted as $\phi_e(x,t)$. We define a debiased electrolyte potential that subtracts out the potential at the negative current collector where $x = 0$: $\tilde{\phi}_e(x,t) = \phi_e(x,t) - \phi_e(0,t)$. Furthermore, we break up $\tilde{\phi}_e(x,t)$ into two parts: $\tilde{\phi}_e(x,t) = [\tilde{\phi}_e(x,t)]_1 + [\tilde{\phi}_e(x,t)]_2$. The transfer function $[\tilde{\Phi}_e(x,s)]_1/I_{app}(s)$ for $x$ locations in the negative electrode is given by Eq. (28). For $x$ locations in the separator, this transfer function is given by Eq. (29), and for $x$ locations in the positive electrode, this transfer function is given by Eq. (30). Once the appropriate $[\tilde{\phi}_e(x,t)]_1$ is computed, we compute $\tilde{\phi}_e(x,t) = [\tilde{\phi}_e(x,t)]_1 + (2RT(1-t_+^0)/F)\ln(c_e(x,t)/c_e(0,t))$, where $c_e(x,t)$ is computed as described in the "concentration in electrolyte" summary item. Finally,

$$\begin{aligned}\phi_{\mathrm{e}}(x,t) &= \tilde{\phi}_{\mathrm{e}}(x,t)+\phi_{\mathrm{e}}(0,t)\\ &= \tilde{\phi}_{\mathrm{e}}(x,t)-\tilde{\phi}_{\mathrm{s-e}}(0,t),\end{aligned}$$

where $\tilde{\phi}_{\mathrm{s-e}}(0,t)$ at $x=0$ is found via the transfer function in Eq. (20) using negative-electrode variables.

**Concentration in electrolyte:** Lithium concentration in the electrolyte is denoted $c_{\mathrm{e}}(x,t)$. We use an eigenfunction expansion to express $c_{\mathrm{e}}(x,t)$ in terms of $K+1$ weighted partial transfer functions, where $K$ is at least as large as the anticipated reduced-order-model system order. The first term of the expansion is the equilibrium concentration so we define $\tilde{c}_{\mathrm{e}}(x,t) = c_{\mathrm{e}}(x,t)-c_{\mathrm{e},0}$ and use the transfer function in Eq. (49) to find $\tilde{C}_{\mathrm{e}}(x,s)/I_{\mathrm{app}}(s)$. Details of finding the eigenfunctions $\Psi(x;\lambda_{\mathrm{k}})$ are given in Section 2.5. The individual partial transfer functions are expressed in Eq. (47). The two parts of this transfer function are found in Eqs. (45) and (46).

## 3. Discrete-time realization algorithm

We have now derived all of the necessary continuous-time transfer functions required to model the internal dynamics of a lithium-ion cell. Proceeding, our goal is to convert these transfer functions into an optimal reduced-order discrete-time state-space model of the form

$$\begin{aligned}\boldsymbol{x}(t+T_s) &= \boldsymbol{A}\boldsymbol{x}(t)+\boldsymbol{B}\boldsymbol{i}_{\mathrm{app}}(t)\\ \boldsymbol{y}(t) &= \boldsymbol{C}\boldsymbol{x}(t)+\boldsymbol{D}\boldsymbol{i}_{\mathrm{app}}(t),\end{aligned}$$

where $T_s$ is the sampling period of the discrete-time ROM, $\boldsymbol{x}(t)$ is the "state" vector of the model at time $t$, $\boldsymbol{y}(t)$ is the "output" vector of the model at time $t$, and $\boldsymbol{A}$, $\boldsymbol{B}$, $\boldsymbol{C}$, and $\boldsymbol{D}$ are matrices. Note that the ROM states and outputs are valid only at values of time that are integer multiples of $T_s$.

The challenge in accomplishing this conversion is that the transfer functions are transcendental in the Laplace variable $s$, which makes closed-form solutions intractable. To overcome this obstacle, we introduced the "discrete-time realization algorithm" (DRA) in the first paper in this series [10]. The DRA relies on the Ho–Kalman algorithm [14], which generates an optimal reduced-order discrete-time state-space realization from a discrete-time system pulse response. Therefore, the DRA first finds the discrete-time pulse response, and then uses the Ho–Kalman algorithm to compute the state-space realization. A summary of the steps implemented by the DRA is given below. A detailed description of the algorithm is given in [10].

1 Sample the continuous-time transfer function in the frequency domain at a high rate $F_s$ (not related to $T_s$), and take the inverse discrete Fourier transform (IDFT) to get an approximation to the continuous-time impulse response.
2 Form the continuous-time step response from the continuous-time impulse response, and then compute the discrete-time pulse response values from the continuous-time step response, assuming a sample and hold circuit connected to the system input.
3 Generate a discrete-time state-space realization using the deterministic Ho–Kalman algorithm. This algorithm returns the reduced-order $\boldsymbol{A}$, $\boldsymbol{B}$, and $\boldsymbol{C}$ matrices from the discrete-time pulse-response sequence in Step 2. The order of the system is determined from the sorted singular values of the Hankel matrix that is computed as part of the algorithm. The $\boldsymbol{D}$ matrix is found by the initial value theorem.
4 Transform the state space system into the desired final form using a similarity transformation, if required.

Note that the transfer function that is being converted from a continuous-time representation to a reduced-order discrete-time state-space realization may be single-input single-output, multi-input single-output, single-input multi-output, or multi-input multi-output. Here, we are considering the case of a single input $i_{\mathrm{app}}(t)$ and multiple outputs, where the outputs comprise the set of transfer functions from Section 2.2 that the user would like to implement. The overall transfer function being implemented by the DRA is then the vertical concatenation of all sub-transfer functions. For example, if the user would like to determine $j(0,t)$ and $\eta(1,t)$, the overall transfer function would be

$$\mathbf{H}(s) = \begin{bmatrix}\dfrac{J(0,s)}{I_{\mathrm{app}}(s)}\\[2ex] \dfrac{\eta(1,s)}{I_{\mathrm{app}}(s)}\end{bmatrix}.$$

Prior to implementing DRA Step 1, $\mathbf{H}(s)$ must be strictly stable (e.g., it may not contain a pole at $s=0$, which corresponds to integration dynamics). If $\mathbf{H}(s)$ has a pole at $s=0$, this pole must first be removed. To do so, we determine the residue associated with this pole using $\boldsymbol{res}_0 = \lim_{s\to 0} s\mathbf{H}(s)$. Then, we run the DRA on the strictly stable system $\mathbf{H}^*(s)$ where $\mathbf{H}^*(s) = \mathbf{H}(s) - \boldsymbol{res}_0/s$. For the transfer functions in Section 2, two have a pole at the origin: the potential difference transfer function (Eq. (20)) and the solid surface concentration transfer function (Eq. (23)). We calculate the residue for these poles and then subtract them out giving,

$$\frac{\tilde{\Phi}^{*}_{\mathrm{s-e}}(z,s)}{I_{\mathrm{app}}(s)} = \frac{\tilde{\Phi}_{\mathrm{s-e}}(z,s)}{I_{\mathrm{app}}(s)} - \frac{\tilde{\phi}^{\mathrm{res0}}_{\mathrm{s-e}}}{s} \tag{50}$$

$$\frac{\tilde{C}^{*}_{\mathrm{s,e}}(z,s)}{I_{\mathrm{app}}(s)} = \frac{\tilde{C}_{\mathrm{s,e}}(z,s)}{I_{\mathrm{app}}(s)} - \frac{\tilde{c}^{\mathrm{res0}}_{\mathrm{s,e}}}{s} \tag{51}$$

where

$$\tilde{\phi}^{\mathrm{res0}}_{\mathrm{s-e}} = \frac{-3\left[\left.\dfrac{\partial U_{\mathrm{ocp}}}{\partial c_{\mathrm{s,e}}}\right|_{c_{\mathrm{s},0}}\right]}{a_{\mathrm{s}}FLAR_{\mathrm{s}}} \tag{52}$$

$$\tilde{c}^{\mathrm{res0}}_{\mathrm{s,e}} = \frac{-3}{a_{\mathrm{s}}FLAR_{\mathrm{s}}}. \tag{53}$$

The superscript asterisk on the transfer function denotes that the transfer function had a pole at the origin that is now removed. We use the transfer functions in Eq. (50) and Eq. (51) instead of Eq. (20) and Eq. (23) as input to the DRA. In the final state space representation, we augment the state-space realization with an integrator state to account for removal of the pole in the DRA. The reduced-order approximation to the original system via the augmented discrete-time state-space model is:

$$\mathbf{x}(t+T_s) = \underbrace{\left[\begin{array}{c:c}\mathbf{A}_{\mathrm{DRA}} & 0\\ \hdashline 0 & 1\end{array}\right]}_{\mathbf{A}_{\mathrm{aug}}}\mathbf{x}(t) + \underbrace{\left[\begin{array}{c}\mathbf{B}_{\mathrm{DRA}}\\ \hdashline T_s\end{array}\right]}_{\mathbf{B}_{\mathrm{aug}}} i_{\mathrm{app}}(t) \tag{54}$$

$$\mathbf{y}(t) = \underbrace{\left[\begin{array}{c:c}\mathbf{C}_{\mathrm{DRA}} & \mathbf{res}_0\end{array}\right]}_{\mathbf{C}_{\mathrm{aug}}}\mathbf{x}(t) + \mathbf{D}\, i_{\mathrm{app}}(t). \tag{55}$$

where $\mathbf{res}_0$ is a column vector containing the residues of the transfer functions with a pole at the origin. The subscript "DRA" on

the ***A***, ***B***, and ***C*** matrices denotes the state space realization computed by Step 3 of the DRA.

The length of the output vector depends on the number of $z$ locations (for the electrode-scale properties) and $x$ locations (for the cell-scale properties) chosen by the user for evaluation. For example, solving for the seven variables $\tilde{\phi}^{*}_{s-e}$, $j$, $\eta$, $\tilde{c}_{s,e}$, $\tilde{\phi}_s$, $[\tilde{\phi}_e]_1$ and $\tilde{c}_e$ at four spatial locations each (e.g., both current collectors and both electrode–separator interfaces) produces a total of 28 outputs. The output $\mathbf{y}(t)$ then has the following structure:

$$\mathbf{y}(t) = \begin{bmatrix} \tilde{\phi}^{*}_{s-e}(z,t) \\ j(z,t) \\ \eta(z,t) \\ \tilde{c}_{s,e}(z,t) \\ \tilde{\phi}_s(z,t) \\ \left[\tilde{\phi}_e(x,t)\right]_1 \\ \tilde{c}_e(x,t) \end{bmatrix},$$

where each variable is a four-vector corresponding to the four spatial locations evaluated.

Note that DRA Step 1 requires we select a high-rate sampling frequency $F_s$ to approximate the impulse response of the continuous-time system. We find that the results are not very sensitive to $F_s$, but that it is important that the duration of the truncated impulse response is long enough to capture the slow time constants in the model.

While the elements of the output vector $y(t)$ of the DRA have physical meaning, the only state variable within the state vector $x(t)$ that has independent physical interpretation is the integrator state. If this state is $x_I(t)$, then we have that the average concentration of lithium in the solid is equal to

$$c_{s,avg}(t) = c_{s,0} + \left(\tilde{c}^{res0}_{s,e}\right)x_I(t).$$

As the average concentration of lithium in an electrode is related to the state-of-charge of the electrode via an affine transformation, the value of the integrator state is key to being able to estimate cell SOC.

## 4. Nonlinear output equations

The reduced-order model produced by the DRA is entirely linear, whereas true cell behavior is nonlinear. In some cases, the nonlinear cell variable is simply an affine function of the linear output, and the nonlinear value is recovered by adding a constant to the linear output. In other cases, the transformation is more complex. This section first shows how to recover the nonlinear internal cell variables from the linear cell variables, then how to estimate the nonlinear cell voltage.

### 4.1. Computing nonlinear internal variables

**Reaction flux:** Outputs $j_{DRA}(z,t)$ from the DRA are a linearized approximation to the true $j(z,t)$. There is no additional correction to this variable.

**Overpotential:** We find that outputs $\eta_{DRA}(z,t)$ from the DRA accurately predict the variability of the true $\eta(z,t)$, but do not always predict the mean of $\eta(z,t)$ well. The average value for $\eta$ across the electrode, based on the linearized model of Section 2, is

$$\overline{\eta}_{linear}(s) = FR_{ct}\int_0^1 \frac{J(z,s)}{I_{app}(s)}I_{app}(s)dz$$

$$\overline{\eta}_{linear}(t) = \frac{R_{ct}}{a_s L_n A}i_{app}(t),$$

for the negative electrode (with a similar result for the positive electrode). If we make the simplifying assumption that reaction flux is approximately uniform across the electrode, then the "correct" nonlinear average can be computed using $\bar{j}(t) = i_{app}(t)/(a_s F L_n A)$ and by inverting the Butler–Volmer equation to find $\overline{\eta}_{nonlinear}$. Substituting $\bar{j}(t)$ for $j(t)$ in Eq. (5) gives

$$i_{app}(t) = a_s F L_n A j_0\left(\exp\left(\frac{(1-\alpha)F}{RT}\overline{\eta}_{nonlinear}\right) - \exp\left(-\frac{\alpha F}{RT}\overline{\eta}_{nonlinear}\right)\right),$$

where $j_0(z,t) = kc_e^{1-\alpha}(c_{max}-c_s)^{1-\alpha}c_s^{\alpha}$ with values of $c_e$ and $c_s$ corresponding to this particular cell location at this point in time. If $\alpha = 0.5$, the "correct" nonlinear average overpotential at a point in the negative electrode is

$$\overline{\eta}_{nonlinear}(z,t) = \frac{2RT}{F}\left(\frac{i_{app}(t)}{2j_0(z,t)a_s F L_n A}\right).$$

The nonlinear corrected $\eta$ is computed by subtracting $\overline{\eta}_{linear}(t)$ from the linear DRA output $\eta_{DRA}(z,t)$, and then by adding $\overline{\eta}_{nonlinear}(z,t)$:

$$\eta(z,t) = \eta_{DRA}(z,t) - \overline{\eta}_{linear}(t) + \overline{\eta}_{nonlinear}(z,t). \quad (56)$$

**Solid surface concentration:** The debiased solid surface concentration variable $\tilde{c}_{s,e}(z,t)$ is defined as $\tilde{c}_{s,e}(z,t) = c_{s,e}(z,t) - c_{s,0}$ (Eq. (12)). Therefore, the value for $c_{s,e}(z,t)$ is found by adding the equilibrium concentration to $\tilde{c}_{s,e}(z,t)$:

$$c_{s,e}(z,t) = \tilde{c}_{s,e}(z,t) + c_{s,0}.$$

**Potential in solid:** The debiased solid potential variable $\tilde{\phi}_s(z,t)$ is defined as $\tilde{\phi}_s(z,t) = \phi_s(z,t) - \phi_s(0,t)$. In the negative electrode, $\phi_s(0,t) = 0$ and in the positive electrode, $\phi_s(0,t) = v(t)$, the cell voltage. Therefore, $\phi_s(z,t) = \tilde{\phi}_s(z,t)$ in the negative electrode and $\phi_s(z,t) = \tilde{\phi}_s(z,t) + v(t)$ in the positive electrode, where the calculation of $v(t)$ is discussed in Section 4.2.

**Concentration in electrolyte:** The electrolyte concentration is approximated by truncating the infinite-series expansion shown in Eq. (49). The equilibrium value is added to the appropriate output of the state space model to arrive at the true value of $c_e(x,t) = \tilde{c}_e(x,t) + c_{e,0}$.

**Solid–Electrolyte potential difference:** The debiased solid–electrolyte potential difference $\tilde{\phi}_{s-e}$ is defined as $\tilde{\phi}_{s-e}(z,t) = \phi_{s-e}(z,t) - U_{ocp}(c_{s,0})$. The corresponding transfer function $\tilde{\Phi}_{s-e}(z,s)/I_{app}(s)$ has a pole at $s = 0$, which is removed to give the $\tilde{\Phi}^{*}_{s-e}(z,s)/I_{app}(s)$ transfer function, which is used within the DRA to produce $\tilde{\phi}^{*}_{s-e}(z,t)$. The integrator response could be added back manually, as in $\tilde{\phi}_{s-e}(t) = \tilde{\phi}^{*}_{s-e}(t) + (\tilde{\phi}^{res0}_{s-e})x_I(t)$, but better performance is obtained by looking deeper at what is actually happening.

Recall that $c_{s,avg}(t) = (\tilde{c}^{res0}_{s,e})x_I(t) + c_{s,0}$ and note that $\tilde{\phi}^{res0}_{s-e} = \left.\frac{\partial U_{ocp}}{\partial c_{s,e}}\right|_{c_{s,0}} \times \tilde{c}^{res0}_{s,e}$. Therefore, we can write

$$\phi_{s-e}(z,t) = \tilde{\phi}^{*}_{s-e}(z,t) + \left(U_{ocp}(c_{s,0}) + \left[\left.\frac{\partial U_{ocp}}{\partial c_{s,e}}\right|_{c_{s,0}}\right](c_{s,avg} - c_{s,0})\right),$$

where the second term on the right-hand side is equal to the first two terms of the Taylor series expansion of $U_{ocp}(c_{s,avg})$ around the starting average concentration $c_{s,0}$. Therefore, instead of implementing $\tilde{\Phi}_{s-e}(z,s)/I_{app}(s)$, we find that we achieve more accurate results if we implement $\tilde{\Phi}^{*}_{s-e}(z,s)/I_{app}(s)$ and then compute

$$\phi_{s-e}(z,t) = \tilde{\phi}^{*}_{s-e}(z,t) + U_{ocp}(c_{s,avg}(t)).$$

**Potential in electrolyte:** As described in Section. 2.4, the electrolyte potential $\phi_e(x,t)$ is comprised of two terms. The first term $[\phi_e(x,t)]_1$ is found using $[\tilde{\phi}_e(x,t)]_1$ which is an output from the DRA:

$$[\phi_e(x,t)]_1 = \left[\tilde{\phi}_e(x,t)\right]_1 + \phi_e(0,t).$$

We use $\phi_e(0,t) = \phi_s(0,t) - \phi_{s-e}(0,t)$ and the fact that $\phi_s(0,t) = 0$ at the negative current collector to get

$$[\phi_e(x,t)]_1 = \left[\tilde{\phi}_e(x,t)\right]_1 - \phi_{s-e}(0,t).$$

The second term in the $\phi_e(x,t)$ equation, $[\tilde{\phi}_e(x,t)]_2$, is given by Eq. (31). The values for $c_e(x,t)$ are outputs of the state space model with the addition of the equilibrium value, as described above. The overall electrolyte potential is given by

$$\phi_e(x,t) = [\phi_e(x,t)]_1 + \frac{2RT(1-t^0_+)}{F}\ln\left(\frac{c_e(x,t)}{c_e(0,t)}\right).$$

### 4.2. Cell voltage

The cell voltage is the difference in solid potential between the two current collectors, $v(t) = \phi_s(L,t) - \phi_s(0,t)$. Using the overpotential equation, $\eta = \phi_s - \phi_e - U_{ocp} - FR_{film}j$ and $\tilde{\phi}_e(x,t) = \phi_e(x,t) - \phi_e(0,t)$ we write

$$\begin{aligned} v(t) &= \phi_s(L,t) - \phi_s(0,t) \\ &= \eta(L,t) + \phi_e(L,t) + U_{ocp}(L,t) + FR_{film,p}j(L,t) - \eta(0,t) \\ &\quad - \phi_e(0,t) - U_{ocp}(0,t) - FR_{film,n}j(0,t) \\ &= (\eta(L,t) - \eta(0,t)) + \tilde{\phi}_e(L,t) + (U_{ocp}(L,t) - U_{ocp}(0,t)) \\ &\quad + F\left(R_{film,p}j(L,t) - R_{film,n}j(0,t)\right). \end{aligned}$$

If we split the $\tilde{\phi}_e(L,t)$ term into its two components, we can write the output as

$$\begin{aligned} v(t) = F\left(R_{film,p}j(L,t) - R_{film,n}j(0,t)\right) + \left[\tilde{\phi}_e(L,t)\right]_1 + (\eta(L,t) \\ - \eta(0,t)) + \left[\tilde{\phi}_e(L,t)\right]_2 + \left(U_{ocp}(c_{s,e}(L,t)) - U_{ocp}(c_{s,e}(0,t))\right). \end{aligned} \quad (57)$$

At first glance, it appears that we require implementing a minimum of nine transfer functions to be able to compute cell voltage: $j(L,t)$, $j(0,t)$, $[\tilde{\phi}_e(L,t)]_1$, $\eta(L,t)$, $\eta(0,t)$, $c_e(L,t)$, $c_e(0,t)$, $c_{s,e}(L,t)$, and $c_{s,e}(0,t)$. However, the linear transfer functions can be grouped together. Define

$$\begin{aligned} \frac{V_{lin}(s)}{I_{app}(s)} = F\left(R_{film,p}\frac{J(L,s)}{I_{app}(s)} - R_{film,n}\frac{J(0,s)}{I_{app}(s)}\right) + \frac{\left[\tilde{\phi}_e(L,s)\right]_1}{I_{app}(s)} \\ + \left(\frac{\eta(L,s)}{I_{app}(s)} - \frac{\eta(0,s)}{I_{app}(s)}\right). \end{aligned}$$

If this transfer function is implemented in the DRA to produce a single output $v_{lin}(t)$, then we can write

$$\begin{aligned} v(t) &= v_{lin}(t) - \overline{\eta}_{linear,p}(t) + \overline{\eta}_{nonlinear,p}(L,t) + \overline{\eta}_{linear,n}(t) \\ &\quad - \overline{\eta}_{nonlinear,n}(0,t) + \left[\tilde{\phi}_e(L,t)\right]_2 + \left(U_{ocp}(c_{s,e}(L,t)) \right. \\ &\quad \left. - U_{ocp}(c_{s,e}(0,t))\right). \end{aligned} \quad (58)$$

**Table 1**
Cell parameters for simulation.

| Symbol | Units | Negative electrode | Separator | Positive electrode |
|---|---|---|---|---|
| $L$ | μm | 128 | 76 | 190 |
| $R$ | μm | 12.5 | – | 8.5 |
| $A$ | $m^2$ | 1 | 1 | 1 |
| $\sigma$ | S $m^{-1}$ | 100 | – | 3.8 |
| $\varepsilon_s$ | $m^3$ $m^{-3}$ | 0.471 | – | 0.297 |
| $\varepsilon_e$ | $m^3$ $m^{-3}$ | 0.357 | 0.724 | 0.444 |
| brug | – | 1.5 | – | 1.5 |
| $c_s^{max}$ | mol $m^{-3}$ | 26,390 | – | 22,860 |
| $c_{e,0}$ | mol $m^{-3}$ | 2000 | 2000 | 2000 |
| $\theta_{i,min}$ | – | 0.05 | – | 0.78 |
| $\theta_{i,max}$ | – | 0.53 | – | 0.17 |
| $D_s$ | $m^2$ $s^{-1}$ | $3.9 \times 10^{-14}$ | – | $1.0 \times 10^{-13}$ |
| $D_e$ | $m^2$ $s^{-1}$ | $7.5 \times 10^{-11}$ | $7.5 \times 10^{-11}$ | $7.5 \times 10^{-11}$ |
| $t^0_+$ | – | 0.363 | 0.363 | 0.363 |
| $k$ | $mol^{-1/2}$ $m^{5/2}$ $s^{-1}$ | $1.94 \times 10^{-11}$ | – | $2.16 \times 10^{-11}$ |
| $\alpha$ | – | 0.5 | – | 0.5 |
| $R_{film}$ | $\Omega m^2$ | 0.0 | – | – |

We compute $\sigma^{eff} = \sigma\varepsilon_s$, $\kappa^{eff} = \kappa\varepsilon_e^{brug}$, $D_e^{eff} = D_e\varepsilon_e^{brug}$
In the electrolyte, conductivity is a function of concentration: $\kappa(c_e) = 4.1253 \times 10^{-2} + 5.007 \times 10^{-4}c_e - 4.7212 \times 10^{-7}c_e^2 + 1.5094 \times 10^{-10}c_e^3 - 1.6018 \times 10^{-14}c_e^4$.
For the negative electrode, the open-circuit potential function is: $U_{ocp}(\theta) = -0.16 + 1.32\exp(-3.0\theta) + 10.0\exp(-2000.0\theta)$.
For the positive electrode, the open-circuit potential function is: $U_{ocp}(\theta) = 4.19{,}829 + 0.0565661\tanh(-14.5546\theta + 8.60942) - 0.0275479\left[\frac{1}{(0.998432-\theta)^{0.4924656}} - 1.90111\right] - 0.157123\exp(-0.04738\theta^6) + 0.810239\exp[-40(\theta - 0.133875)]$.

This output equation requires implementing a minimum number of five transfer functions to be able to compute cell voltage: $v_{lin}(t)$, $c_e(L,t)$, $c_e(0,t)$, $c_{s,e}(L,t)$, and $c_{s,e}(0,t)$.

## 5. Simulation and results

In this section, we use simulation to demonstrate the performance of the reduced-order model as compared to the full-order PDEs describing the porous-electrode model. The parameters of the cell being simulated are those published by Doyle et al. [15], and are listed in Table 1. The cell input current for the simulation is based on the Environmental Protection Agency's (EPA) Urban Dynamometer Driving Schedule (UDDS), which was developed by the EPA to represent city driving conditions for light duty vehicles. Fig. 2 shows the normalized UDDS profile of current versus time, as computed for a medium-size electric vehicle. For our simulations we multiplied this profile by two, to achieve a maximum absolute rate of 2C, which for this cell corresponds to 41 A.

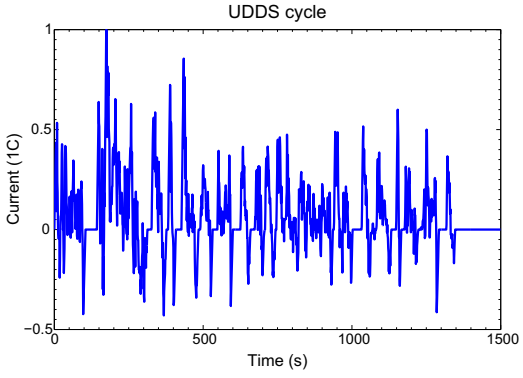


**Fig. 2.** Normalized profile of cell current versus time for the UDDS cycle.

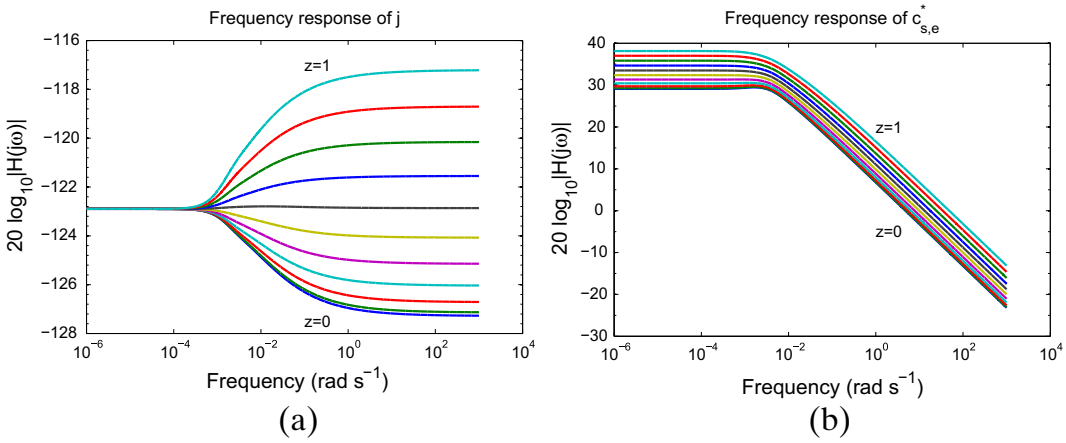


**Fig. 3.** Frequency response of two internal cell variables at locations within the negative electrode.

We compare our ROM results to simulations of the pseudo-2D porous-electrode model, which we implemented in COMSOL Multiphysics version 4.2a. We implemented two different versions of the porous-electrode model: (1) a "rigorous PDE" version, which implements Eqs. (1)–(6) as listed, and (2) a "linearized PDE" version, which linearizes the PDEs of Eqs. (1)–(6) to exactly match Assumptions 1 and 2. Specifically, the linearized PDE model is created from the rigorous PDE model with the following modifications: (1) the $U_{ocp}$ functions are linearized about the initial cell SOC, (2) the second term of Eq. (15) is dropped, (3) the value of $\kappa$ remains constant throughout the simulation, at the value corresponding to the initial electrolyte concentration, and (4) we use the linearized Butler–Volmer equation with the $j_0$ term constant throughout the simulation. Because these same assumptions are made to generate the ROM, we expect that ROM solution will converge to the linearized PDE model as we increase the order of the ROM.

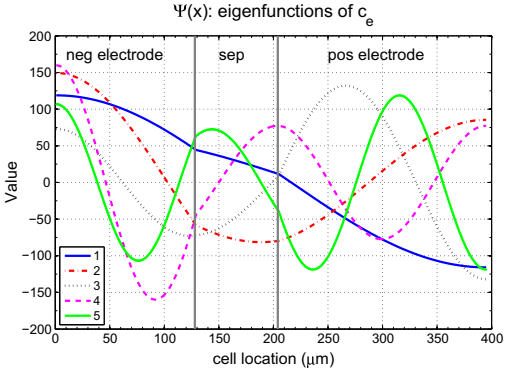


**Fig. 4.** Eigenfunctions used in the computation of electrolyte concentration.

In all cases, the simulation is initialized with a cell SOC of 60%. We compute DRA outputs and PDE outputs for all seven cell variables ($\phi_{s-e}$, $\eta$, $j$, $c_{s,e}$, $\phi_s$, $\phi_e$, and $c_e$) at four different spatial locations across the cell (at both current collectors, and at both electrode/separator interfaces). The reduced-order state-space model therefore has one input (cell current) and 28 outputs.

Fig. 3 shows the frequency responses for two of the continuous-time transfer functions. The reaction flux is shown in Frame (a) which is a plot of Eq. (21) at $z$ locations ranging from 0 to 1 at 0.1 increments. The surface concentration, with the pole at $s = 0$ removed (Eq. (51)), is plotted in Frame (b) at the same $z$ locations. We see that although the transfer functions are mathematically complex, the frequency response of the variables is actually quite simple. This is why a reduced-order model can accurately approximate the rigorous PDE model.

When approximating the electrolyte concentration, we use eigenvalue/eigenfunction pairs $\lambda_k$ and $\Psi(x;\lambda_k)$ for $n = 0,\ldots,5$. The "zeroth" eigenvalue/eigenfunction simply gives the equilibrium

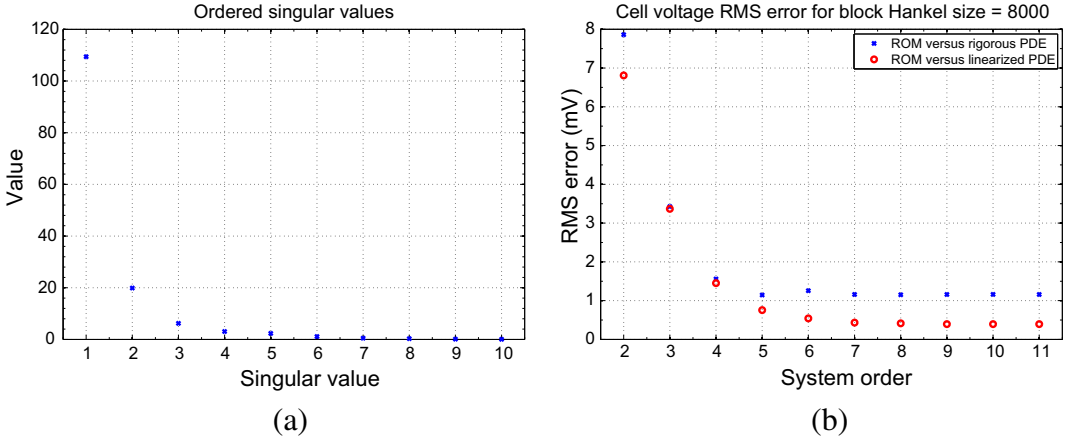


**Fig. 5.** Singular values in DRA step 3 for a Hankel matrix size of 8000, and RMS voltage prediction errors for different system orders.

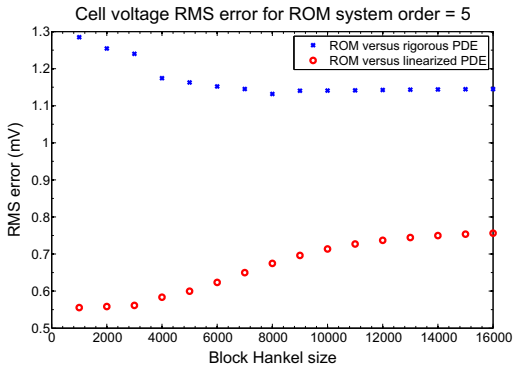


**Fig. 6.** RMS voltage prediction errors for different Hankel matrix sizes in DRA step 3.

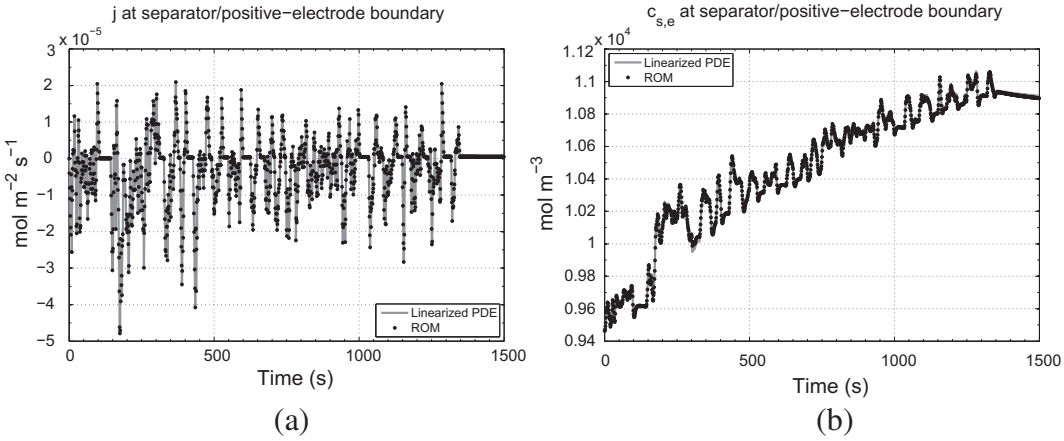


**Fig. 7.** Comparison of ROM to linearized PDE model.

concentration ($c_{e,0} = 2000$ mol m$^{-3}$) and is therefore not included in the state-space model explicitly. Fig. 4 plots eigenfunctions $\Psi(x;\lambda_k)$ for $n = 1,\ldots5$.

Four tuning parameters must be set to generate a cell model using the DRA: the high-rate sampling frequency $F_s$ for Step 1 of the DRA, the size of the Hankel matrix for Step 3 of the DRA, the number of states in the reduced-order system, and the sampling period $T_s$ of the computed discrete-time reduced-order model. For the simulation runs presented in this paper, the high-rate sampling frequency was chosen as $F_s = 128$ Hz and the sampling period of the computed discrete-time reduced-order model was chosen as $T_s = 1$s. The computational complexity required to run the DRA and the accuracy of the resulting reduced-order model predictions are not sensitive to either of these parameters.

We use the ordered singular values of the system Hankel matrix in Step 3 of the DRA to indicate the relative importance of each state, to assist in determining the best tradeoff between final ROM complexity and fidelity. Fig. 5(a) shows the first ten singular values. The tradeoff between accuracy and complexity is application dependent but it is evident that there is no need to include any more than the sixth singular value (which is about 1% of the first singular value). The root-mean-squared (RMS) error between the PDE simulation and the ROM simulation of cell voltage as a function of the system order is shown in Fig. 5(b).[4] We see that the RMS error between the ROM and the linearized PDE model approaches zero, and that the RMS error between the ROM and the rigorous PDE model approaches a constant value. In both cases, we achieve little improvement in RMS error after about the fifth state. Thus, from now on, we use a ROM having exactly five state variables in its state vector $x(t)$.

The final DRA tuning parameter is the length of the discrete-time pulse response included in the Hankel matrix. This value must be large enough to capture the extent of the longest pulse response (slowest system dynamics) which turn out to be that of the surface concentration of lithium in the positive electrode. Fig. 6 shows that the cell voltage RMS error is fairly invariant to the block Hankel matrix size, although we find that the fidelity of individual transfer functions can be sensitive to this value, and larger lengths usually help.

Based on these results, we generate a ROM having five states using a Hankel matrix block size of 8000. Fig. 7 compares the reaction flux and the solid surface concentration of the ROM to the linearized PDE model. Although the figure shows results for only two of the 28 outputs, the other 26 match similarly well. This indicates that we can reduce the infinite-order system to a fifth-order system with high accuracy.

Results of comparing this ROM to the rigorous PDE model at the electrode/separator interfaces are presented in Fig. 8. The electrochemical reactions at the electrode/separator interface are more dynamic than at the current collectors and are therefore more difficult for the ROM to match. Of particular interest are the results for the reaction flux (Frames (a) and (b)) where

[4] Note the system order in this plot includes the addition of the augmented integrator term.

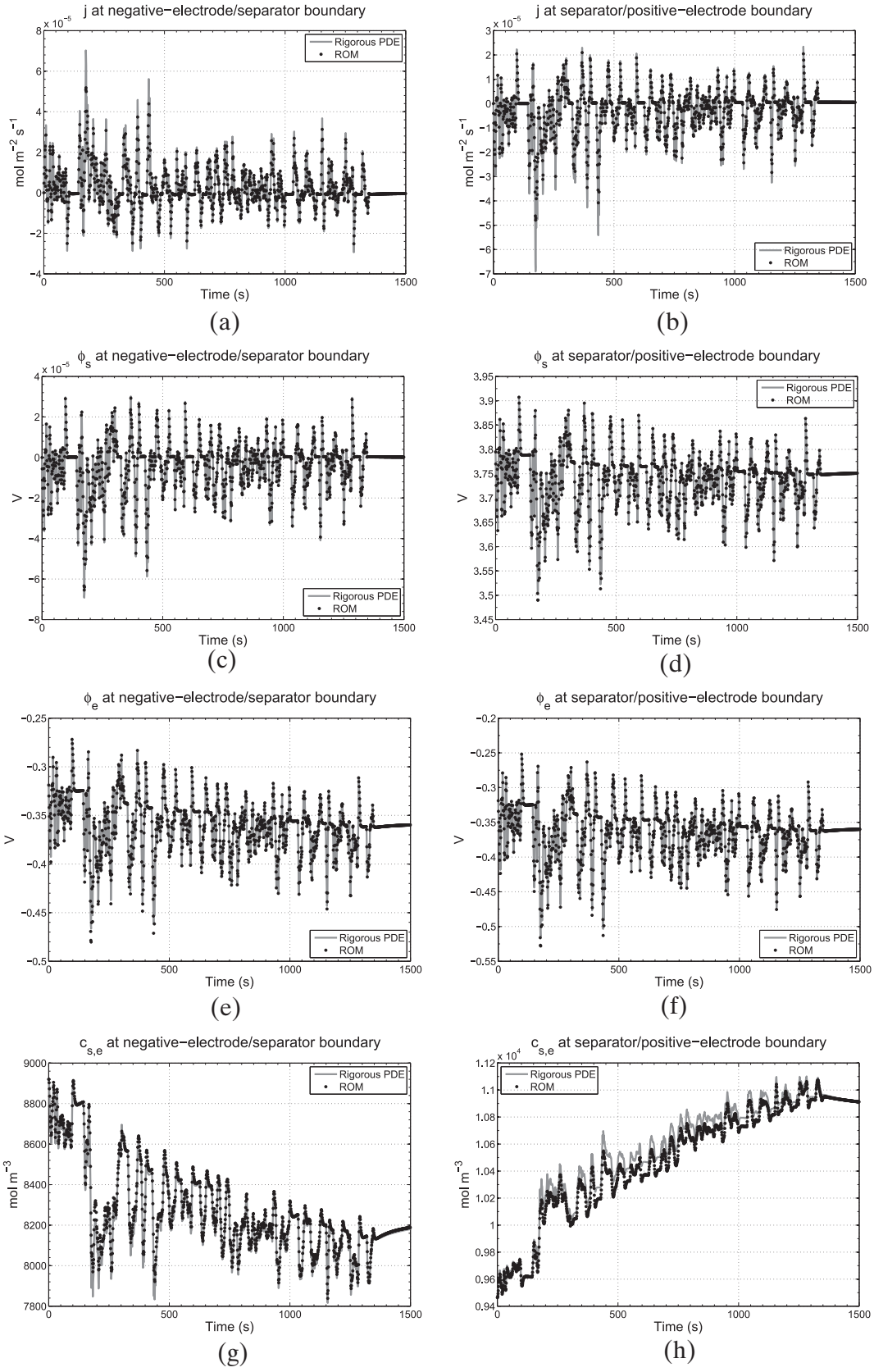


**Fig. 8.** Comparison of the fifth-order ROM to the rigorous PDE cell model.

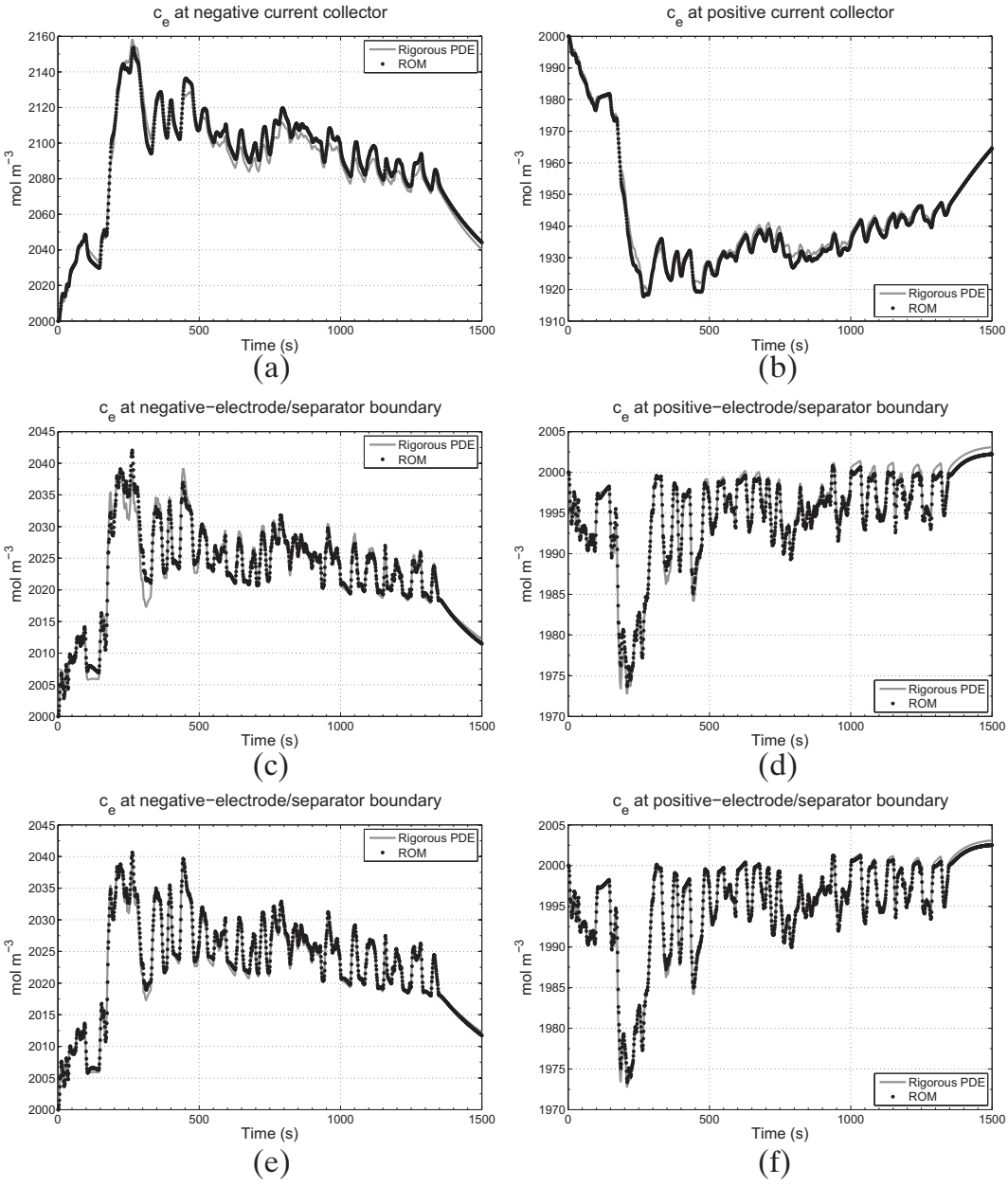


**Fig. 9.** Comparison of the fifth-order ROM to the rigorous PDE cell model for $c_e$ (eighth-order ROM for e,f).

the ROM does not match the rigorous PDE model especially well at highly dynamic times (e.g., near $t = 170$ s). We attribute this error to the assumptions made in linearizing the full-order model. The rigorous PDE model predicts a higher dynamic response than does the linearized PDE model, which can be seen by comparing Fig. 8(b) and Fig. 7(a). The same effect is seen with the surface lithium concentration at the positive electrode/separator boundary which is shown in Fig. 8(h). Again the ROM predicts the linearized PDE response extremely well as shown in Fig. 7(b), but the linearized PDE model and the rigorous PDE model differ.

Increasing the model order or increasing the size of the Hankel matrix does not improve modeling of $j$ or $c_{s,e}$ because the ROM already matches the linearized PDE model. However, unlike $j$ or $c_{s,e}$, the results for the electrolyte concentration can be improved by increasing the system order. The infinite-series expansion used to represent the electrolyte concentration is truncated in the ROM. Increasing the number of states results in slightly better estimation of $c_e$. Fig. 9(a–d) shows the comparison between the fifth-order ROM and the rigorous PDE model. Fig. 9(e,f) shows the concentration at the separator interface with an eighth-order ROM.

The output cell voltage for the ROM is calculated from the electrochemical variables using Eq. (57). The results of the fifth-order ROM and the rigorous PDE model are shown in Fig. 10. The cell voltage RMS error between the rigorous PDE model and the ROM is 1.14 mV. Frame (b) shows a detailed view of the simulation during the period of the greatest mismatch. Frame (c) illustrates the difference between the corrected and uncorrected $\eta$ value, as

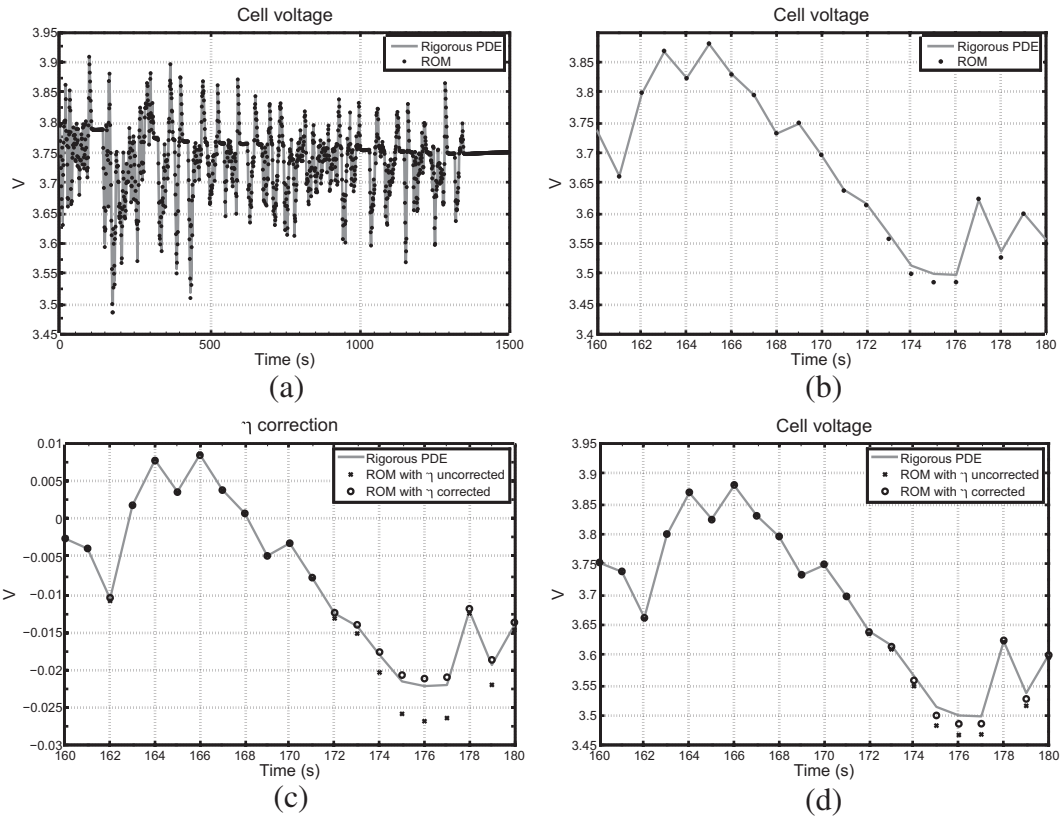


**Fig. 10.** Comparing ROM to rigorous PDE model for cell voltage.

**Table 2**
ROM for five states, to compute output voltage only.

$$\boldsymbol{A}=\begin{bmatrix} 0.7568 & 0 & 0 & 0 & 0 \\ 0 & 0.9840 & 0 & 0 & 0 \\ 0 & 0 & 0.9969 & 0 & 0 \\ 0 & 0 & 0 & 0.9998 & 0 \\ 0 & 0 & 0 & 0 & 1.0000 \end{bmatrix}, \boldsymbol{B}=\begin{bmatrix} 1 \\ 1 \\ 1 \\ 1 \\ 1 \end{bmatrix}, \boldsymbol{D}=\begin{bmatrix} -7.333\times10^{-3} \\ 0 \\ 0 \\ 0 \end{bmatrix},$$

$$\boldsymbol{C}=\begin{bmatrix} -6.459\times10^{-5} & -7.214\times10^{-6} & -1.280\times10^{-6} & -3.572\times10^{-7} & 0 \\ 3.489\times10^{-2} & 2.861\times10^{-2} & -8.019\times10^{-2} & -7.194\times10^{-4} & 0 \\ -1.287\times10^{-1} & 3.944\times10^{-2} & 1.149\times10^{-1} & -1.171\times10^{-3} & 0 \\ 5.569\times10^{-1} & 3.514\times10^{-2} & 9.591\times10^{-3} & -9.381\times10^{-2} & 1.837\times10^{-1} \\ -1.300\times10^{+0} & -2.369\times10^{-1} & -3.840\times10^{-2} & 1.692\times10^{-3} & -1.719\times10^{-1} \end{bmatrix}$$

discussed in Section. 4, over the same period and Frame (d) shows this impact on the cell voltage.

The fifth-order ROM used in these simulations has 28 linear outputs. In general, the cell voltage calculation itself requires only five linear outputs. Table 2 shows the A, B, C, and D matrices for a minimum-output fifth-order reduced-order model that can be used to calculate cell output voltage. The input is $i_{\text{app}}(t)$, and the output is

$$y(t) = \begin{bmatrix} v_{\text{lin}}(t) \\ \tilde{c}_{\text{e}}(L,t) \\ \tilde{c}_{\text{e}}(0,t) \\ \tilde{c}_{\text{s,e}}(L,t) \\ \tilde{c}_{\text{s,e}}(0,t) \end{bmatrix}.$$

Eq. (58) can be used to turn these five linear outputs into a nonlinear voltage estimate. Simulations using this minimum-output fifth-order reduced-order model match those shown in Fig. 10.

## 6. Conclusions

In this paper we have developed a one-dimensional physics-based reduced-order model for lithium-ion cells. To do so, we first augmented the set of electrochemical-variable transfer functions developed by Smith et al. [8,9] with transfer functions for the solid and electrolyte potentials $\phi_{\text{s}}$ and $\phi_{\text{e}}$, and the electrolyte concentration $c_{\text{e}}$. The discrete-time realization algorithm is used to produce an optimal reduced-order discrete-time state-space model from these transfer functions, overcoming the limitations of nonlinear optimization approaches. Nonlinear corrections to the linearized model are also given to improve accuracy of the method.

The final state-space ROM used in Section. 5 requires 134 msec to simulate the 1500 s UDDS profile on a desktop computer, which is about 0.09 msec sample$^{-1}$. In contrast, the rigorous model, which is run using COMSOL, requires almost 13 min (or 510 msec sample$^{-1}$) for the same simulation on the same desktop computer. This is a speedup of over 5000:1. Thus, we conclude that the simplicity of the ROM makes it feasible for use in real-time control applications such as in electric-vehicle battery-management systems.

Note that a change in parameter values, such as happens during cell aging, does not change the transfer-function equations of the model developed in Section. 2; however, the state-space reduced-order model will need to be regenerated from these transfer functions using the DRA discussed in Section. 3. The DRA requires about 11 min on the same desktop computer to generate the reduced-order model from the transfer functions. (Again, this process must be performed only (1) once to create the original ROM from the original set of parameters, and (2) whenever the

parameter values are deemed to have changed significantly from their original values—perhaps once per month of regular operation, and when it can be performed during an interval when the BMS is otherwise essentially idle, as might be the case when the battery pack is being charged.) We note that the extended time required to calculate the ROM when parameter values are modified makes it impractical for use in system-identification applications.

Finally, the results show that a fifth-order ROM is able to track the highly dynamic UDDS profile of current versus time with an output cell voltage root-mean-squared error of less than 1.2 mV for the specific cell parameters considered. This ROM also tracks all of the cell's electrochemical states at any position across its cross section with a high degree of accuracy. The greatest source of mismatch between the ROM and PDE simulation predictions arises as a result of the linearization assumptions made when creating the transfer functions of the model. As the cell state moves away from from the initial linearization set-point, prediction errors also increase. In a future paper we will discuss a method to overcome this limitation.

## Acknowledgment

Financial support for the research reported in this paper has been received from Texas Instruments.

## References

[1] X. Hu, S. Li, H. Peng, Journal of Power Sources 198 (2012) 359–367.
[2] M. Doyle, T.F. Fuller, J. Newman, Journal of the Electrochemical Society 140 (1993) 1526–1533.
[3] T.F. Fuller, M. Doyle, J. Newman, Journal of the Electrochemical Society 141 (1994) 1–10.
[4] C. Wang, W.B. Gu, B. Liaw, Journal of the Electrochemical Society 145 (1998) 3407–3417.
[5] V.R. Subramanian, V.D. Diwakar, D. Tapriyal, Journal of the Electrochemical Society 152 (2005) A2002–A2008.
[6] J.C. Forman, S. Bashash, J.L. Stein, H.K. Fathy, Journal of the Electrochemical Society 158 (2011) A93–A101.
[7] L. Cai, R.E. White, Journal of the Electrochemical Society 156 (2009) A154–A161.
[8] K. A. Smith, Electrochemical Modeling, Estimation and Control of Lithium Ion Batteries, Ph.D. thesis, Pennsylvania State University, 2006.
[9] K.A. Smith, C.D. Rahn, C.-Y. Wang, Energy Conversion and Management 48 (2007) 2565–2578.
[10] J.L. Lee, A. Chemistruck, G.L. Plett, Journal of Power Sources 206 (2012) 367–377.
[11] T. Jacobsen, K. West, Electrochimica Acta 40 (1995) 255–262.
[12] A.P. Schmidt, M. Bitzer, Á.W. Imre, L. Guzzella, Journal of Power Sources 195 (2010) 7634–7638.
[13] R.P. Agarwal, D. O'Regan, An Introduction to Ordinary Differential Equations, Universitext, Springer, New York, 2008, pp. 28–34.
[14] B.L. Ho, R.E. Kalman, Regelungstechnik 14 (1966) 545–548.
[15] M. Doyle, J. Newman, A.S. Gozdz, C.N. Schmutz, J.-M. Tarascon, Journal of the Electrochemical Society 143 (1996) 1890–1903.

## Nomenclature[5]

$A$: surface area of the electrode, $m^2$
$\boldsymbol{A}$: state transition matrix of the state-space model
$a_s$: specific surface area of the porous electrode, $m^2\ m^{-3}$
$\boldsymbol{B}$: input matrix of the state-space model
$\boldsymbol{C}$: output matrix of the state-space model
$c$: concentration of lithium in phase indicated by subscript, mol $m^{-3}$
$c_{e,0}$: steady-state concentration of lithium in the electrolyte phase, mol $m^{-3}$
$c^*_{e,k}$: $k$th generalized Fourier coefficient of $c_e(x,t)$
$c_{max}$: maximum lithium concentration in an electrode particle, mol $m^{-3}$
$c_{s,0}$: initial concentration of lithium in the solid phase, mol $m^{-3}$
$c_{s,avg}$: average concentration of lithium in an electrode particle, mol $m^{-3}$
$c_{s,e}$: surface concentration of lithium in a spherical electrode particle, mol $m^{-3}$
$\bar{c}_{s,e}$: debiased version of $c_{s,e}$, $\bar{c}_{s,e} = c_{s,e} - c_{s,0}$, mol $m^{-3}$
$\boldsymbol{D}$: input–output coupling matrix of the state-space model
$D_e^{eff}$: effective electrolyte diffusivity, $m^2\ s^{-1}$
$D_s$: solid diffusivity, $m^2\ s^{-1}$
$f_{\pm}$: mean molar activity coefficient
$F$: Faraday's constant, 96 487 C $mol^{-1}$
$F_s$: sampling frequency of the transfer functions in DRA Step 1
$I$: applied current density, A $m^{-2}$
$i_{app}$: applied cell current, $i_{app} = IA$, A
$i_e$: ionic current, A $m^{-2}$
$j$: reaction flux, mol $m^{-2}\ s^{-1}$
$j^*_k$: $k^{th}$ generalized Fourier coefficient of $j(x,t)$
$k$: rate constant for the electrochemical reaction, $mol^{\alpha-1}m^{4-3\alpha}s^{-1}$
$L$: (without subscript) length of the cell, m
$L$: (with subscript) length of region of cell, m
$T_s$: sampling period of final discrete-time state space system, s
$r$: radial coordinate, m
$\boldsymbol{res}_0$: residues of poles of transfer functions at $s = 0$
$R$: universal gas constant, 8.31451 J $mol^{-1}\ K^{-1}$
$R_{ct}$: charge transfer resistance, $\Omega\ m^2$
$R_{film}$: film resistance, $\Omega\ m^2$
$R_s$: particle radius, m
$R_{tot}$: sum of the charge transfer resistance and the film resistance, $\Omega\ m^2$
$T$: temperature, K
$t^0_+$: transference number
$t$: time, s
$U_{ocp}$: open circuit potential, V
$v$: cell voltage, V
$x$: lD linear coordinate across the cell, m
$\boldsymbol{x}$: state of state-space model
$\boldsymbol{y}$: linear output of state-space model
$z$: unitless dimension across electrode

*Greek*
$\alpha$: charge-transfer coefficient
$\beta$: parameter of Jacobsen–West transfer function: $\beta = R_s s/D_s$
$\varepsilon$: volume fraction of phase indicated by subscript
$\phi$: potential of the phase indicated by subscript, V
$\bar{\phi}$: debiased potential of the phase indicated by subscript, V
$\phi_{s-e}$: potential difference between solid and electrolyte phases, V
$[\phi_e]_1$: linear part of $\phi_e$, V
$[\phi_e]_2$: nonlinear part of $\phi_e$, V
$\eta$: local overpotential, V
$\kappa^{eff}$: effective electrolyte conductivity, S $m^{-1}$
$\lambda_k$: $k^{th}$ eigenvalue of the electrolyte concentration function
$\nu$: non-spatial-dependent ODE coefficient, dimensionless
$\Psi$: eigenfunction of the electrolyte concentration function
$\sigma^{eff}$: effective solid conductivity, S $m^{-1}$

*Subscript/superscript*
$e$: pertaining to the electrolyte phase
$m$: pertaining to the separator ("middle" of cell)
$k$: pertaining to the negative electrode
$p$: pertaining to the positive electrode
$s$: pertaining to the solid phase

[5] Unless otherwise specified, lowercase symbols correspond to constants or time-domain quantities; uppercase symbols correspond to Laplace frequency-domain quantities.